



THE UNIVERSITY *of* EDINBURGH

Edinburgh Research Explorer

Signatures of TOP1 transcription-associated mutagenesis in cancer and germline

Citation for published version:

Reijns, MAM, Parry, DA, Williams, TC, Nicholson, MD, Carroll, P, Ridout, K, The Genomics England Research Consortium, Colorectal Cancer Domain UK 100,000 Genomes Project, Schuh, A, Aden, K, Palles, C, Campo, E, Stankovic, T, Taylor, MS & Jackson, AP 2022, 'Signatures of TOP1 transcription-associated mutagenesis in cancer and germline', *Nature*. <https://doi.org/doi: 10.1038/s41586-022-04403-y>

Digital Object Identifier (DOI):

[doi: 10.1038/s41586-022-04403-y](https://doi.org/doi: 10.1038/s41586-022-04403-y)

Link:

[Link to publication record in Edinburgh Research Explorer](#)

Document Version:

Peer reviewed version

Published In:

Nature

Publisher Rights Statement:

Open Access This article is licensed under a Creative Commons Attribution 4.0 International License, which permits use, sharing, adaptation, distribution and reproduction in any medium or format, as long as you give appropriate credit to the original author(s) and the source, provide a link to the Creative Commons license, and indicate if changes were made. The images or other third party material in this article are included in the article's Creative Commons license, unless indicated otherwise in a credit line to the material. If material is not included in the article's Creative Commons license and your intended use is not permitted by statutory regulation or exceeds the permitted use, you will need to obtain permission directly from the copyright holder. To view a copy of this license, visit <http://creativecommons.org/licenses/by/4.0/>.

General rights

Copyright for the publications made accessible via the Edinburgh Research Explorer is retained by the author(s) and / or other copyright owners and it is a condition of accessing these publications that users recognise and abide by the legal requirements associated with these rights.

Take down policy

The University of Edinburgh has made every reasonable effort to ensure that Edinburgh Research Explorer content complies with UK legislation. If you believe that the public display of this file breaches copyright please contact openaccess@ed.ac.uk providing details, and we will remove access to the work immediately and investigate your claim.



1 Signatures of TOP1 transcription-associated mutagenesis in cancer and 2 germline

3 Martin A.M. Reijns^{1,14*}, David A. Parry^{1,14}, Thomas C. Williams^{1,2,14}, Ferran Nadeu^{3,4}, Rebecca L.
4 Hindshaw⁵, Diana O. Rios Szwed¹, Michael D. Nicholson⁶, Paula Carroll¹, Shelagh Boyle⁷, Romina
5 Royo⁸, Alex J. Cornish⁹, Hang Xiang¹⁰, Kate Ridout¹¹, The Genomics England Research Consortium⁺,
6 Colorectal Cancer Domain UK 100,000 Genomes Project⁺, Anna Schuh¹¹, Konrad Aden¹⁰, Claire
7 Palles⁵, Elias Campo^{3,4,12,13}, Tatjana Stankovic⁵, Martin S. Taylor^{2*}, Andrew P. Jackson^{1*}

8

9 ¹ Disease Mechanisms, MRC Human Genetics Unit, Institute of Genetics and Cancer, The University
10 of Edinburgh, Edinburgh, UK

11 ² Biomedical Genomics, MRC Human Genetics Unit, Institute of Genetics and Cancer, The University
12 of Edinburgh, Edinburgh, UK

13 ³ Institut d'Investigacions Biomèdiques August Pi i Sunyer (IDIBAPS), Barcelona, Spain

14 ⁴ Centro de Investigación Biomédica en Red de Cáncer (CIBERONC), Madrid, Spain

15 ⁵ Institute of Cancer and Genomic Sciences, University of Birmingham, Edgbaston, UK

16 ⁶ Cancer Research UK Edinburgh Centre, Institute of Genetics and Cancer, The University of
17 Edinburgh, Edinburgh, UK

18 ⁷ Genome Regulation, MRC Human Genetics Unit, Institute of Genetics and Cancer, The University of
19 Edinburgh, Edinburgh, UK

20 ⁸ Barcelona Supercomputing Center (BSC), Barcelona, Spain

21 ⁹ The Institute of Cancer Research, London, UK

22 ¹⁰ Institute of Clinical Molecular Biology, Christian-Albrechts-University and University Hospital
23 Schleswig-Holstein, Kiel, Germany

24 ¹¹ Department of Oncology, University of Oxford, Oxford, UK

25 ¹² Hospital Clínic of Barcelona, Barcelona, Spain

26 ¹³ Departament de Fonaments Clínics, Universitat de Barcelona, Barcelona, Spain

27 ¹⁴ These authors contributed equally: Martin A.M. Reijns, David A. Parry, Thomas C. Williams

28 ⁺ A list of authors and their affiliations appears at the end of the paper.

29

30 ^{*} Correspondence to MAMR, MST, APJ

31 **Abstract**

32 The mutational landscape is shaped by many processes, with genic regions vulnerable to mutation
33 but preferentially protected by transcription-coupled repair¹. In microbes, transcription has been
34 demonstrated to be mutagenic^{2,3}; however, the impact of transcription-associated mutagenesis
35 remains to be established in higher eukaryotes⁴. Here we show that ID4, an indel cancer signature of
36 unknown aetiology⁵ characterised by short deletions (2-5 bp), is due to a transcription-associated
37 mutagenesis process. We demonstrate defective ribonucleotide excision repair in mammals to be
38 associated with the ID4 signature, with mutations occurring at a TNT sequence motif, implicating
39 Topoisomerase 1 (TOP1) activity at sites of genome-embedded ribonucleotides as a mechanistic
40 basis. Such TOP1-mediated deletions occur somatically in cancer, and the ID-TOP1 signature is also
41 found in physiological settings, contributing to genic *de novo* indel mutations in the germline. Hence,
42 while topoisomerases protect against genome instability by releasing topological stress⁶, their
43 activity may also be an important source of mutations in the human genome.

44 **Introduction**

45 Eukaryotic cells employ many strategies to ensure integrity of their genomes, with high-fidelity DNA
46 replication⁷ and DNA repair processes countering exogenous and endogenous DNA lesions⁸. The
47 process of transcription targets DNA repair machinery to expressed genes, preferentially reducing
48 their mutation rate following DNA damage¹. Despite this targeted repair, in micro-organisms the
49 process of transcription itself is mutagenic; a phenomenon referred to as transcription-associated
50 mutagenesis (TAM)^{2,3}. In yeast, Topoisomerase 1 (Top1) activity is a major source of TAM and results
51 in a distinctive transcription-dependent signature of 2-5 bp deletions at tandem repeat sequences⁹⁻
52 ¹¹. Genome-embedded ribonucleotides have been established as a cause of Top1-TAM deletions in
53 yeast¹². Such ribonucleotides are frequently incorporated by DNA polymerases during replication,
54 and represent the most prevalent aberrant nucleotides in the eukaryotic genome^{13,14}. These
55 genome-embedded ribonucleotides are normally removed by ribonucleotide excision repair (RER), a
56 process initiated by the heterotrimeric Ribonuclease H2 enzyme¹⁵. However, when Top1 cleaves at
57 embedded ribonucleotides instead of RNase H2 this can result in small deletions^{16,17}.

58 In the last decade, widespread use of genome sequencing has enabled unbiased sampling of human
59 mutations, substantially advancing understanding of mutagenesis in the germline¹⁸ and in
60 neoplasia¹⁹. Multiple mutational processes act during cancer evolution, and mathematical methods
61 have been developed to define signatures that may correspond to individual mutagenic
62 mechanisms, through decomposition of tumour mutational profiles¹⁹. This has successfully defined
63 cell-intrinsic, environmental and treatment-related origins for many base substitution signatures in
64 cancer²⁰⁻²². However, the origin of a substantial number of signatures remains unknown, and some
65 may be artefactual. Recently, cancer signature analysis has been extended to indels⁵, small (1-49 bp)
66 insertions and deletions. Such indels are an important class of mutations that contribute
67 substantially to disease-causing germline variants (>20%) and human variation²³.

68 Here we investigate an indel signature of unknown cause, ID4. We show experimentally that ID4
69 deletions are increased in RNase H2 deficient cell lines and cancers and delineate a human TOP1-
70 mediated TAM signature (ID-TOP1) relevant to both somatic and germline mutagenesis.

71

72 **Results**

73 **ID4, a distinct cancer indel signature**

74 The ID4 cancer signature, as categorised by COSMIC²⁴, comprises 2-5 bp deletions, often with loss of
75 a single repeat unit at short repeat sequences⁵. Most commonly these occur where the deleted
76 sequence is repeated one, two or three times in tandem (Fig. 1a). Hereafter we use the term SSTRs
77 (short-short tandem repeats) to distinguish such short tandem repeats (STRs) with less than 5
78 repeats (i.e. <6 repeat units) from microsatellite STRs with many repeats. In addition to these SSTR
79 deletions, ID4 is characterised by small deletions at sequences with microhomology (MH), in
80 particular 2 bp deletions with single nucleotide microhomology (SNMH). Both features are distinct
81 from cancer deletion signatures resulting from other well-recognised mechanisms like replication
82 slippage and non-homologous/microhomology-mediated end joining (NHEJ/MMEJ) (Extended Data
83 Fig. 1a,b). In support of a distinct aetiology, SSTR and SNMH deletions are not apparent in cancer
84 associated with homologous recombination (HR) or mismatch repair (MMR) deficiency, which are
85 expected to have higher levels of MMEJ and replication slippage mutagenesis, respectively
86 (Extended Data Fig. 1c,d).

87

88 **ID4 resembles a yeast mutation signature**

89 Noting similarities to a Top1-induced transcription-associated mutagenesis (Top1-TAM) in
90 *Saccharomyces cerevisiae*, we re-analysed published genome-wide mutation accumulation
91 experiments performed with *rnh201Δ pol2-M644G* yeast²⁵. This strain is particularly susceptible to

92 Top1-TAM as it accumulates genome-embedded ribonucleotides at high levels due to RNase H2/RER
93 deficiency and enhanced ribonucleotide incorporation by a steric-gate mutation in the catalytic site
94 of the replicative polymerase Pol ϵ ²⁶. Similarities to the ID4 signature were apparent with a
95 comparable pattern of small deletions at SSTRs, although mutational events at sites of SNMH were
96 not evident in the yeast data (Fig. 1b). As over one million ribonucleotides are incorporated by DNA
97 polymerases per replicating mouse cell¹⁴, we reasoned that genome-embedded ribonucleotides
98 might cause similar mutational events in mammalian cells. To experimentally address whether TAM
99 contributes to indel formation in human RER-deficient cells, we developed a novel reporter to
100 enable sensitive and specific detection of mutational events arising from TOP1 activity in both yeast
101 and mammals.

102

103 **Top1-dependent deletions in yeast**

104 Mutation rates are routinely measured in *S. cerevisiae* using well characterised but species-specific
105 selectable markers (LYS2, URA3, CAN1). Therefore, to establish a system that could be transferred
106 between yeast and mammalian cells, we used an approach inspired by the Traffic Light reporter
107 assay²⁷, incorporating both positive and negative selection cassettes in a single transcriptional unit
108 (Fig. 1c). The hygromycin resistance gene (HygroR) served both as the mutational target and
109 negative selection marker. Indels causing a 2 bp frameshift within HygroR, including 2 bp deletions,
110 result in translation of an otherwise out-of-frame P2A self-cleaving peptide and the neomycin
111 resistance (NeoR) gene, permitting positive selection of mutated colonies with neomycin (Extended
112 Data Fig. 2a). To enrich the target for 2 bp tandem repeats, *in silico* re-design incorporated
113 synonymous substitutions such that SSTRs accounted for >50% of the HygroR open reading frame.
114 For validation, the reporter was inserted into the *S. cerevisiae* genome and fluctuation assays used
115 to assess mutation rates in strains deficient for RER and/or Top1. A 37-fold increase in mutation rate
116 was seen for the *rnh201Δ* (RNase H2 null) strain compared to wild type (Fig. 1d), with a mutation

117 rate of 6.1×10^{-9} per bp per generation (95% CI, 5.4 - 6.9×10^{-9}), whereas the increased mutation rate
118 was abolished in the *rnh201Δ top1Δ* double mutant strain, in keeping with Top1-dependent
119 mutagenesis at genome-embedded ribonucleotides^{12,28}. Notably, there was a 10-fold decrease in the
120 mutation rate for *top1Δ* compared to the wild-type strain, and a 35-fold decrease in 2 bp SSTR
121 deletions (Extended Data Fig. 2b), consistent with previous reports^{10,11}. In addition, the observed
122 mutational spectrum was most similar for wild-type and *rnh201Δ* strains, but substantially different
123 compared to *top1Δ* and *rnh201Δ top1Δ* strains (Fig. 1e; Extended Data Fig. 2c-f). Taken together, we
124 conclude that the same Top1-mediated mutations occur, albeit at different frequencies, in wild-type
125 cells when RER is functional and in RNase H2 deficient strains when elevated levels of
126 ribonucleotides are present in the genome.

127

128 **TOP1-mediated mutations in human cells**

129 Having validated the reporter in yeast, the same 2 bp repeat-enriched HygroR sequence was used to
130 address whether TOP1-mediated mutagenesis at embedded ribonucleotides is conserved in human
131 cells (Fig. 2; Extended Data Fig. 2g). NeoR was replaced by the puromycin resistance (PuroR) gene,
132 with reporter expression driven from the mammalian ubiquitous CAG promoter, permitting rapid
133 antibiotic selection in mammalian cells. This modified reporter was inserted at the *AAVS1* safe
134 harbour locus in HeLa cells (Fig. 2a; Extended Data Fig. 3a-e). CRISPR/Cas9-mediated genome
135 editing, targeting the catalytic site of *RNASEH2A*, was then used to generate two independent
136 knockout (KO) reporter clones, alongside a control clone that had also been taken through editing
137 and clonal selection steps (Fig 2b,c; Extended Data Fig. 3). The control clone retained RNase H2
138 activity, while there was complete loss of cellular RNase H2 activity in KO clones, accompanied by
139 high levels of ribonucleotides in genomic DNA (Fig. 2b,c; Extended Data Fig. 3f,g).

140 In fluctuation assays, RNase H2 null clones demonstrated a significant 3.1-fold increase in mutation
141 rate (Fig. 2d) and 5.2-fold more 2 bp SSTR deletions (Extended Data Fig. 3h) compared with RNase

142 H2 proficient cells (RNASEH2A+), consistent with conservation of TOP1-directed mutagenesis in
143 human cells. As in yeast (Fig. 1e), the overall mutational profile of reporter mutations was similar
144 between RNase H2 proficient and null HeLa cells (cosine similarity 0.89, $P < 10^{-4}$), predominantly
145 comprised of 2 bp SSTR deletions (Fig. 2e).

146 The mutation rate for RNase H2 null HeLa cells (8.0×10^{-9} per bp per generation; 95% CI, $6.7-9.5 \times 10^{-9}$)
147 was similar to that seen for *rnh201Δ* yeast (Fig. 1d), whereas the rate was substantially higher for
148 RNASEH2A+ control cells compared to wild-type yeast. However, the increased mutation rate in
149 RNase H2 null HeLa cells likely underestimates the true impact of RER deficiency in human cells, as
150 despite the control RNASEH2A+ HeLa reporter cells retaining protein expression (Fig. 2b), the clone
151 had also acquired mutations at the CRISPR editing site that reduced enzymatic activity (Fig 2c),
152 causing a moderate increase in genomic ribonucleotide content (Extended Data Fig. 3f,g).

153 To confirm these findings we used a complementary approach to establish the relevance of such
154 mutational events genome-wide, performing mutation accumulation experiments using hTERT-RPE1
155 (*TP53*^{-/-}) diploid cell lines. Ancestral populations for RNase H2 wild-type and null cells (RNASEH2A-
156 KO or RNASEH2B-KO; Extended Data Fig. 4a-d) were established after initial single cell sorting, and
157 clones then grown for approximately 100 generations. Single cell sorting was performed every 25
158 generations, creating bottlenecks to capture accumulating mutations (Fig. 3a). Combined variant
159 calling on whole genome sequencing (WGS) from paired ancestral and endpoint cultures identified a
160 total of 1,698 acquired high confidence indel mutations, captured by at least 3 out of 4 variant
161 callers. Consistent with TOP1-mediated mutagenesis, among all indel categories, only 2-5 bp
162 deletions were found to be substantially (7.4-fold) and significantly enriched in RNase H2 null RPE1
163 cells compared to wild-type (Fig. 3b; Extended Data Fig. 4e,f), with an estimated rate of 1.1×10^{-10} 2-5
164 bp deletions per generation per bp for KO and 1.4×10^{-11} for WT. Of these deletions in RNase H2 null
165 cells, 82% were 2 bp deletions, of which 48% were at SSTRs (Extended Data Fig. 4g). Furthermore,
166 signature decomposition using SigProfilerExtractor⁵ reported a 21% ID4 contribution in RNase H2

167 null cells, that increased to 61% when subtraction of background mutation patterns was performed
168 to identify RER-deficiency specific mutation signatures (Fig. 3c,d; Extended Data Fig. 5). The ID4
169 signature was substantially enriched in transcribed genomic regions (Extended Data Fig. 5e). ID5, a
170 clock-like signature⁵, was also enriched in KO cells, likely due to slower growth and longer culture
171 time needed to achieve the same number of doublings for RNase H2 null cells¹⁴.

172

173 **MH deletions specific to mammalian TOP1**

174 Small deletions at sequences with microhomology are an additional feature of ID4 (Fig. 1a), not
175 observed in *rnh201Δ pol2-M644G* yeast (Fig. 1b). However, consistent with a ribonucleotide-induced
176 mutational origin in mammalian cells, they are observed frequently in RNase H2-deficient RPE1 cells,
177 in which SNMH sites account for 31% of 2 bp deletions, indicating that in humans they share the
178 same aetiology as those occurring at SSTRs. Taken together, our reporter and mutation
179 accumulation experiments demonstrate that genome-embedded ribonucleotides cause a similar
180 mutational signature in yeast and mammalian cells. Therefore Topoisomerase 1-mediated
181 mutagenesis likely also occurs in humans and is associated with 2-5 bp deletions at SSTR and SNMH
182 sequences.

183

184 **ID4 mutations in a murine cancer model**

185 To determine if TOP1-induced mutations resulting in the ID4 signature can be detected *in vivo*, we
186 next studied an RER-deficient murine cancer model in which Villin-Cre conditional deletion of
187 *Rnaseh2b* and *Tp53* results in intestinal malignancy²⁹. Whole genome sequencing of paired tumour-
188 normal tissue samples from 6 mice, identified a total of 989 high-confidence tumour-specific somatic
189 indels. Analysis of the resulting mutational signature established that ID4 substantially contributed in
190 all tumours (Fig. 4a,b and Extended Data Fig. 6a), accounting for 32% of acquired indels. Consistent

191 with a transcription-associated process, the ID4 signature was again most evident in transcribed
192 genomic regions (Fig. 4b). Commonly occurring cancer signatures⁵ ID1, ID2 and ID5 were also seen,
193 in line with expectations of multiple mutational processes active in neoplasia.

194 The observed ID4 mutation spectrum corresponded closely to that seen in the RPE1 mutation
195 accumulation experiment: 28% of indels were at 2-5 bp deletions, of which the majority were again
196 2 bp deletions (82%) predominantly at SSTRs (51%) and sites of SNMH (34%) (Extended Data Fig.
197 6b,c). This is consistent with the occurrence of TOP1-induced somatic mutations at genome-
198 embedded ribonucleotides *in vivo*, conserved across different tissue and cellular contexts, and
199 shows that it can be detected in a cancer setting.

200

201 **A sequence motif for ID4 mutations**

202 While COSMIC defines the ID4 signature on the basis of indel size and repeat/microhomology
203 context (Fig. 1a), the number of indels in the murine RER-deficient tumour model permitted us to
204 further investigate the characteristics of mammalian Topoisomerase 1-induced mutations. We
205 focussed our analysis on 2 bp deletions, as such events represented 81% of >1 bp deletions in the
206 context of tandem repeats and 85% of deletions in sequences with microhomology.

207 First, we classified all 2 bp deletions at STR/SNMH sequences into 6 non-redundant dinucleotide
208 classes, grouping together complementary sequences (Fig. 4c). We noted that the deleted
209 sequences substantially deviated from genome-wide frequencies, with a complete absence of CC/GG
210 and CG/GC deletions, as well as an overrepresentation of the CT category (containing CT, TC, GA and
211 AG deletions). All observed deletions therefore included at least one thymidine (T), which
212 functionally could be accounted for by the very strong preference of mammalian Topoisomerase 1
213 to cleave at a phosphodiester bond with a T immediately upstream³⁰.

214 Next, to investigate the wider sequence context, we aligned sequences containing all 228 two bp
215 deletions (Extended Data Fig. 6e), which indicated that deletions preferentially occur when T
216 nucleotides are spaced at a 2-base interval. Indeed, this TNT motif was present in 100% of SNMH
217 ($n=77$) and STR sites ($n=124$), providing a common unifying sequence context for both deletion types
218 (Fig. 4d), a finding replicated in both our RPE1 (Extended Data Fig. 6e) and yeast datasets (Extended
219 Data Fig. 7). We found TNT to be substantially overrepresented at deletions sites compared to the
220 genome-wide null expectation. Furthermore, while the TNT motif is common at tandem repeat
221 sequences, 2 bp deletions at this motif are still significantly enriched when considering the
222 occurrence of 2 bp STR and SNMH sequences in mouse and human genomes (Fig. 4e; Extended Data
223 Fig. 6f), and STR sequences in the yeast genome (Extended Data Fig. 7).

224 To account for thymidines spaced at a 2-base interval and the occurrence of mammalian SNMH
225 deletions, we developed a revised model based on the established strand realignment model for
226 yeast Top1-mediated mutagenesis^{12,16,17}. In this “TNT model”, TOP1 cleaves preferentially 3’ of an
227 embedded ribouridine, with nucleophilic attack by the 2’-OH of the ribose ring resulting in TOP1
228 release and formation of a non-ligatable nick with a terminal 2’,3’-cyclic phosphate (Fig. 4f, i-iii). This
229 then provides a substrate for TOP1 cleavage 2 bp or more upstream¹⁷, preferentially at a
230 thymidine³⁰. When this second cleavage event happens at a base identical to that of the first cleaved
231 nucleotide, an event more likely at STR and microhomology sequences, strand realignment can then
232 occur, resulting in a nick permissive to religation and TOP1cc reversal (Fig. 4f, iv-vi). An alternative
233 mechanism of sequential Top1 cleavage, in which double-strand breaks occur due to nicking of
234 opposite strands³¹ could not be reconciled with our TNT model, but may account for deletions
235 occurring at non-STR/SNHM sites. Within the TNT motif, deletions were most common at CT and GT
236 dinucleotides in both mammals and yeast (Fig. 4c; Extended Data Fig. 6 and 7b,e), which may be
237 explained, at least in part, by preferential incorporation of ribouridine at CT and GT dinucleotides
238 (Extended Data Fig. 7f and ³²).

239

240 Implicating TOP1-TAM as the cause of the ID4 signature permits us to include additional features in
241 the definition of this COSMIC signature, namely preference for a TNT sequence motif at 2 bp
242 deletion sites and enrichment in transcribed genes. Hereafter, we refer to this extended definition as
243 ID-TOP1. To establish the relevance of the ID-TOP1 signature for human disease and genetic
244 variation, we next examined publicly available datasets.

245

246 **ID-TOP1 in human cancer**

247 *RNASEH2B* is frequently deleted in human cancer, in particular in chronic lymphocytic leukaemia
248 (CLL) given its proximity to a tumour suppressor locus, the *DLEU2-mir-15-16* microRNA cluster³³.
249 Such RNase H2 deficient human cancers should therefore be enriched for the ID4/ID-TOP1 signature.
250 We analysed whole genome sequencing data for 348 CLL patients from two independent
251 cohorts^{34,35}, stratified on *RNASEH2B* deletion status. Somatic variant calling identified a significant
252 increase in 2-5 bp deletions in RNase H2 null tumours (Fig. 5a), while other indels were equally
253 represented across wild-type, heterozygous and null categories (Extended Data Fig. 8a). Of the 2-5
254 bp deletions in tumours with biallelic *RNASEH2B* loss more than half (57%) were 2 bp deletions,
255 which were predominantly at STR and SNMH sequences and substantially enriched for the TNT motif
256 (Extended Data Fig. 8b,c), consistent with the ID-TOP1 mutational signature. Furthermore,
257 mutational signature decomposition for RNase H2 null CLL cases confirmed the presence of the ID4
258 signature, most apparent in genic regions (Extended Data Fig. 8d). We therefore conclude that the
259 ID-TOP1 signature is present in human cancer and enriched in tumours that are RNase H2 deficient.
260 Topoisomerase 1 also causes mutations in RER proficient cells (Fig. 1d-f and ^{10,11}), and therefore is
261 likely to cause mutations in other cancers, with deletions expected to occur most frequently in highly
262 transcribed genes⁴. Accordingly, analysis of WGS data across cancer types (ICGC/PCAWG)
263 demonstrated that the 2-5 bp deletion rate correlates with expression levels of ubiquitously

264 expressed genes (Pearson's $r = 0.86$; $P = 0.0014$), with deletions markedly elevated in the most highly
265 expressed genes (Fig. 5b), in line with previous reports of such deletions in certain cancer genes^{36,37}.
266 Examination of 2 bp deletions (42% of 2-5 bp deletions) across cancer types also demonstrated them
267 to be predominantly in STR and SNMH contexts (Extended Data Fig. 8f) and enriched for the TNT
268 sequence motif (Fig. 5c). Furthermore, using a dataset of TOP1 cleavage events captured by TOP1-
269 seq³⁸, we found 2-5 bp deletions increase in frequency with TOP1 enzymatic activity, with such
270 deletions more prevalent in regions of high TOP1 activity (Fig. 5d). Likewise, TOP1-ID deletion rates
271 also corresponded to TOP1 activity and transcription level, in contrast to all other deletions
272 (Extended Data Fig. 8g,h). Taken together, this establishes a significant role for TOP1-mediated
273 mutagenesis in the generation of somatic deletions.

274 To further explore the role of transcription in deletion mutagenesis of cancer genomes, we identified
275 genes that are highly expressed, but only in certain tissues. For prostate adenocarcinoma, highly
276 expressed prostate-restricted genes were significantly enriched for 2-5 bp deletion mutations
277 compared to other genes in this cancer type, as well as the same genes in other cancers (two-tailed
278 Fisher's exact test, OR 3.5, $P = 2.5 \times 10^{-8}$ after Bonferroni correction; Extended Data Fig. 8i).
279 Importantly, this analysis considers the same sets of genes between cancer types and therefore rules
280 out sequence composition biases as a confounder for elevated ID-TOP1 mutagenesis in highly
281 expressed genes. Extending this approach in an all-versus-all comparison between 8 cancer types
282 and 17 tissues demonstrated specificity between high expression in a tissue of origin and enrichment
283 for 2-5 bp deletions (Fig. 5e). These results extend the relevance of TOP1-mediated mutagenesis to
284 other cancers, confirms the ID-TOP1 mutational signature to be transcription-associated, and
285 supports the occurrence of TAM in humans.

286

287 **TOP1-mediated deletions in the germline**

288 TOP1 is ubiquitously expressed, so we reasoned that it could cause germline as well as somatic
289 mutations. To investigate this possibility we examined mutations from parent-child trio WGS studies
290 in the Gene4Denovo database³⁹. *De novo* mutations identified in such datasets represent germline
291 events, as they occur in germ cells or during early embryonic cell divisions. Strikingly, 2-5 bp
292 deletions were the largest category identified, accounting for 33% of the 40,936 *de novo* indels (Fig.
293 5f), and the majority of these were compatible with the ID-TOP1 signature. Analysis of 2 bp deletions
294 (41% of 2-5 bp deletions) demonstrated that most occur at SSTR or MH sites (Extended Data Fig.
295 9a,b), with enrichment of the TNT sequence motif both genome wide and in the context of
296 STR/SNMH sites (Fig. 5g; Extended Data Fig. 9c). Likewise for 3 and 4 bp deletions, TNNT and TNNNT
297 motifs respectively were significantly overrepresented compared to genome-wide expectation
298 (Extended Data Fig. 9d), in support of sequential TOP1 cleavage and strand realignment as the
299 underlying cause. Consistent with TOP1-TAM aetiology, 2-5 bp deletion and ID-TOP1 deletion
300 frequency correlated with transcript expression in male germ cells (Fig. 5h and Extended Data Fig.
301 9e). We therefore conclude that the ID-TOP1 mutational signature also occurs in the human
302 germline, implicating TOP1-induced strand realignment mutagenesis as an important mutational
303 process in mammalian cells.

304

305 Discussion

306 Here we establish a biological basis for the ID4 cancer signature⁵, experimentally demonstrating it to
307 occur in RNase H2 deficient cells both *in vitro* and *in vivo*. This implicates TOP1-mediated cleavage at
308 genome-embedded ribonucleotides as its cause. TOP1 is cell-essential in mammals, and it is
309 therefore not possible to similarly confirm a genetic dependency on TOP1 in human cells, as has
310 been done in yeast¹². However, conservation of this mechanism across eukaryotes is supported by
311 us finding a Topoisomerase 1 dependent TNT deletion motif present in both yeast and humans, and
312 demonstrating that deletion frequency is dependent on human TOP1 activity levels. Previously

313 published work also provides evidence for TOP1-mutagenesis at ribonucleotide sites in humans. The
314 reversible transesterification reaction of Type 1 Topoisomerases is conserved from yeast to
315 humans⁶, and human TOP1 has site-specific activity for ribonucleotides⁴⁰, causing DNA breaks in
316 mammalian RNase H2 deficient cells³³. Furthermore, generation of 2 bp deletions through sequential
317 TOP1 cleavage at embedded ribonucleotides has been biochemically reconstituted with both human
318 and yeast enzymes^{17,31}.

319 We define additional features of this ID-TOP1 mutational signature, with deletions strongly enriched
320 at TNT motifs in both yeast and mammals, a sequence context specific to Topoisomerase 1
321 ([Extended Data Fig. 7g,h](#)), and deletions most frequent in highly transcribed regions. Consequently,
322 we show that a transcription-associated mutagenesis process first identified in yeast^{10,12,41} is relevant
323 to higher eukaryotes, establishing TOP1-induced mutagenesis as an important process for human
324 variation and disease. Additional signatures associated with topoisomerases or indeed RNase H2
325 may be identified in future, particularly given that ID17 has been recently been linked to TOP2A^{K743N}
326 cancers⁴².

327 The substantial contribution of ID-TOP1 deletions to germline mutagenesis has particular
328 significance given that such deletions will be disproportionately disruptive, particularly in transcribed
329 regions. Notably, such deletions occur in the context of normal RER function, consistent with the
330 mutagenic potential of Topoisomerase 1 in physiological wild-type settings ([Fig. 1d](#) and ^{10,11}). Given
331 that genome-embedded ribonucleotides are the most common endogenous lesion in replicating
332 mammalian cells¹⁴, they are the most likely sites of TOP1-TAM mutagenesis, where TOP1 could
333 cleave before their removal by RNase H2-dependent RER. Processing of TOP1cc may be an
334 alternative, less frequent source of 2-5 bp deletions⁴¹, but we did not detect ID4 in Topoisomerase 1
335 inhibitor treated cancers ([Extended Data Fig. 8j](#)). TOP1 canonical function is to relieve DNA
336 topological stress, arising during both transcription and replication⁶ ([Extended Data Fig. 10](#)). Hence
337 TOP1-mediated deletions are not restricted to transcribed regions of the genome, with deletions

338 also evident in non-genic regions with high TOP1 activity ([Extended Data Fig. 8k](#)). However, overall,
339 enhanced TOP1 activity associated with transcription accounts for more frequent mutagenesis
340 within genes.

341 Given the essential nature of topoisomerase activity across tissues and cell states, TOP1-mediated
342 mutagenesis is likely to occur in many contexts. Frequent TOP1-mediated human germline
343 mutations ([Fig. 5i-k](#)) and identification of ID4 at early embryonic stages⁴³ suggest developmental
344 vulnerability to TOP1-TAM. In addition, 2-5 bp somatic deletions at SSTRs are also observed at high
345 frequency in non-dividing neurons³⁶, and ID4 has been identified in multiple tumour types⁵. As such,
346 this mutational process is likely to be significant not only in cancers with RER deficiency, but also
347 those with high TOP1 activity and tumours with defects in relevant repair mechanisms, such as
348 enzymes that process TOP1cc⁶ or non-ligatable TOP1-induced nicks⁴⁴⁻⁴⁶. In addition, alternative RER
349 pathways may exist⁴⁷ that could reduce TOP1-mutagenesis. The ID-TOP1 signature may provide a
350 useful biomarker with potential future diagnostic and therapeutic utility⁴⁸, for instance as an
351 indicator of TOP1-induced genome instability targetable by PARP or ATR inhibitors^{33,49}.

352 In conclusion, alongside its essential role in relieving DNA torsional stress, TOP1 also drives
353 mutagenesis in somatic and germline contexts, relevant to neoplasia, inherited disease and human
354 variation.

355

356 **References**

357 1 Hanawalt, P. C. & Spivak, G. Transcription-coupled DNA repair: two decades of progress and
358 surprises. *Nat Rev Mol Cell Biol* **9**, 958-970, doi:10.1038/nrm2549 (2008).
359 2 Datta, A. & Jinks-Robertson, S. Association of increased spontaneous mutation rates with
360 high levels of transcription in yeast. *Science* **268**, 1616-1619, doi:10.1126/science.7777859
361 (1995).
362 3 Herman, R. K. & Dworkin, N. B. Effect of gene induction on the rate of mutagenesis by ICR-
363 191 in Escherichia coli. *J Bacteriol* **106**, 543-550, doi:10.1128/JB.106.2.543-550.1971 (1971).
364 4 Jinks-Robertson, S. & Bhagwat, A. S. Transcription-associated mutagenesis. *Annu Rev Genet*
365 **48**, 341-359, doi:10.1146/annurev-genet-120213-092015 (2014).

- 366 5 Alexandrov, L. B. *et al.* The repertoire of mutational signatures in human cancer. *Nature* **578**,
367 94-101, doi:10.1038/s41586-020-1943-3 (2020).
- 368 6 Pommier, Y., Sun, Y., Huang, S. N. & Nitiss, J. L. Roles of eukaryotic topoisomerases in
369 transcription, replication and genomic stability. *Nat Rev Mol Cell Biol* **17**, 703-721,
370 doi:10.1038/nrm.2016.111 (2016).
- 371 7 Kunkel, T. A. Evolving views of DNA replication (in)fidelity. *Cold Spring Harb Symp Quant Biol*
372 **74**, 91-101, doi:10.1101/sqb.2009.74.027 (2009).
- 373 8 Ciccia, A. & Elledge, S. J. The DNA damage response: making it safe to play with knives. *Mol*
374 *Cell* **40**, 179-204, doi:10.1016/j.molcel.2010.09.019 (2010).
- 375 9 Lippert, M. J., Freedman, J. A., Barber, M. A. & Jinks-Robertson, S. Identification of a
376 distinctive mutation spectrum associated with high levels of transcription in yeast. *Mol Cell*
377 *Biol* **24**, 4801-4809, doi:10.1128/MCB.24.11.4801-4809.2004 (2004).
- 378 10 Lippert, M. J. *et al.* Role for topoisomerase 1 in transcription-associated mutagenesis in
379 yeast. *Proceedings of the National Academy of Sciences* **108**, 698-703,
380 doi:10.1073/pnas.1012363108 (2011).
- 381 11 Takahashi, T., Burguiere-Slezak, G., Auffret Van Der Kemp, P. & Boiteux, S. Topoisomerase 1
382 provokes the formation of short deletions in repeated sequences upon high transcription in
383 *Saccharomyces cerevisiae*. *Proceedings of the National Academy of Sciences of the United*
384 *States of America* **108**, 692-697, doi:10.1073/pnas.1012582108 (2011).
- 385 12 Kim, N. *et al.* Mutagenic processing of ribonucleotides in DNA by yeast topoisomerase I.
386 *Science (New York, N.Y.)* **332**, 1561-1564, doi:10.1126/science.1205016 (2011).
- 387 13 Nick McElhinny, S. A. *et al.* Abundant ribonucleotide incorporation into DNA by yeast
388 replicative polymerases. *Proceedings of the National Academy of Sciences of the United*
389 *States of America* **107**, 4949-4954, doi:10.1073/pnas.0914857107 (2010).
- 390 14 Reijns, M. A. M. *et al.* Enzymatic removal of ribonucleotides from DNA is essential for
391 mammalian genome integrity and development. *Cell* **149**, 1008-1022,
392 doi:10.1016/j.cell.2012.04.011 (2012).
- 393 15 Sparks, J. L. *et al.* RNase H2-Initiated Ribonucleotide Excision Repair. *Molecular Cell* **47**, 980-
394 986, doi:10.1016/j.molcel.2012.06.035 (2012).
- 395 16 Huang, S. Y., Ghosh, S. & Pommier, Y. Topoisomerase I alone is sufficient to produce short
396 DNA deletions and can also reverse nicks at ribonucleotide sites. *J Biol Chem* **290**, 14068-
397 14076, doi:10.1074/jbc.M115.653345 (2015).
- 398 17 Sparks, J. L. & Burgers, P. M. Error-free and mutagenic processing of topoisomerase 1-
399 provoked damage at genomic ribonucleotides. *The EMBO journal* **34**, 1259-1269 (2015).
- 400 18 Rahbari, R. *et al.* Timing, rates and spectra of human germline mutation. *Nat Genet* **48**, 126-
401 133, doi:10.1038/ng.3469 (2016).
- 402 19 Alexandrov, L. B. & Stratton, M. R. Mutational signatures: the patterns of somatic mutations
403 hidden in cancer genomes. *Curr Opin Genet Dev* **24**, 52-60, doi:10.1016/j.gde.2013.11.014
404 (2014).
- 405 20 Alexandrov, L. B. *et al.* Signatures of mutational processes in human cancer. *Nature* **500**,
406 415-421, doi:10.1038/nature12477 (2013).
- 407 21 Nik-Zainal, S. *et al.* The genome as a record of environmental exposure. *Mutagenesis* **30**,
408 763-770, doi:10.1093/mutage/gev073 (2015).
- 409 22 Pich, O. *et al.* The mutational footprints of cancer therapies. *Nat Genet* **51**, 1732-1740,
410 doi:10.1038/s41588-019-0525-5 (2019).
- 411 23 Eichler, E. E. Genetic Variation, Comparative Genomics, and the Diagnosis of Disease. *New*
412 *England Journal of Medicine* **381**, 64-74, doi:10.1056/NEJMra1809315 (2019).
- 413 24 Tate, J. G. *et al.* COSMIC: the Catalogue Of Somatic Mutations In Cancer. *Nucleic Acids Res*
414 **47**, D941-D947, doi:10.1093/nar/gky1015 (2019).
- 415 25 Conover, H. N. *et al.* Stimulation of Chromosomal Rearrangements by Ribonucleotides.
416 *Genetics* **201**, 951-961, doi:10.1534/genetics.115.181149 (2015).

417 26 Nick McElhinny, S. A. *et al.* Genome instability due to ribonucleotide incorporation into DNA. *Nature chemical biology* **6**, 774-781, doi:10.1038/nchembio.424 (2010).
418
419 27 Certo, M. T. *et al.* Tracking genome engineering outcome at individual DNA breakpoints. *Nat*
420 *Methods* **8**, 671-676, doi:10.1038/nmeth.1648 (2011).
421 28 Williams, J. S. *et al.* Topoisomerase 1-mediated removal of ribonucleotides from nascent
422 leading-strand DNA. *Molecular cell* **49**, 1010-1015, doi:10.1016/j.molcel.2012.12.021 (2013).
423 29 Aden, K. *et al.* Epithelial RNase H2 Maintains Genome Integrity and Prevents Intestinal
424 Tumorigenesis in Mice. *Gastroenterology* **156**, 145-159.e119,
425 doi:10.1053/j.gastro.2018.09.047 (2019).
426 30 Tanizawa, A., Kohn, K. W. & Pommier, Y. Induction of cleavage in topoisomerase I c-DNA by
427 topoisomerase I enzymes from calf thymus and wheat germ in the presence and absence of
428 camptothecin. *Nucleic Acids Res* **21**, 5157-5166, doi:10.1093/nar/21.22.5157 (1993).
429 31 Huang, S. N., Williams, J. S., Arana, M. E., Kunkel, T. A. & Pommier, Y. Topoisomerase I-
430 mediated cleavage at unrepaired ribonucleotides generates DNA double-strand breaks.
431 *EMBO J* **36**, 361-373, doi:10.15252/embj.201592426 (2017).
432 32 Balachander, S. *et al.* Ribonucleotide incorporation in yeast genomic DNA shows preference
433 for cytosine and guanosine preceded by deoxyadenosine. *Nat Commun* **11**, 2447,
434 doi:10.1038/s41467-020-16152-5 (2020).
435 33 Zimmermann, M. *et al.* CRISPR screens identify genomic ribonucleotides as a source of
436 PARP-trapping lesions. *Nature* **559**, 285-289, doi:10.1038/s41586-018-0291-z (2018).
437 34 Consortium, T. G. E. R. The 100,000 Genomes Project | Genomics England. (2020).
438 35 Puente, X. S. *et al.* Non-coding recurrent mutations in chronic lymphocytic leukaemia.
439 *Nature* **526**, 519-524, doi:10.1038/nature14666 (2015).
440 36 Abascal, F. *et al.* Somatic mutation landscapes at single-molecule resolution. *Nature*,
441 doi:10.1038/s41586-021-03477-4 (2021).
442 37 Rheinbay, E. *et al.* Analyses of non-coding somatic drivers in 2,658 cancer whole genomes.
443 *Nature* **578**, 102-111, doi:10.1038/s41586-020-1965-x (2020).
444 38 Baranello, L. *et al.* RNA Polymerase II Regulates Topoisomerase 1 Activity to Favor Efficient
445 Transcription. *Cell* **165**, 357-371, doi:10.1016/j.cell.2016.02.036 (2016).
446 39 Zhao, G. *et al.* Gene4Denovo: an integrated database and analytic platform for de novo
447 mutations in humans. *Nucleic acids research* **48**, D913--D926 (2020).
448 40 Sekiguchi, J. & Shuman, S. Site-specific ribonuclease activity of eukaryotic DNA
449 topoisomerase I. *Mol Cell* **1**, 89-97, doi:10.1016/s1097-2765(00)80010-6 (1997).
450 41 Cho, J. E., Kim, N., Li, Y. C. & Jinks-Robertson, S. Two distinct mechanisms of Topoisomerase
451 1-dependent mutagenesis in yeast. *DNA Repair (Amst)* **12**, 205-211,
452 doi:10.1016/j.dnarep.2012.12.004 (2013).
453 42 Boot, A. & Rozen, S. G. Recurrent mutations in topoisomerase 2a cause a novel mutator
454 phenotype in human cancers. *bioRxiv* (2020).
455 43 Park, S. *et al.* Clonal dynamics in early human embryogenesis inferred from somatic
456 mutation. *bioRxiv*, 2020.2011.2023.395244, doi:10.1101/2020.11.23.395244 (2020).
457 44 Alvarez-Quilon, A. *et al.* Endogenous DNA 3' Blocks Are Vulnerabilities for BRCA1 and BRCA2
458 Deficiency and Are Reversed by the APE2 Nuclease. *Mol Cell* **78**, 1152-1165 e1158,
459 doi:10.1016/j.molcel.2020.05.021 (2020).
460 45 Li, F. *et al.* Apn2 resolves blocked 3' ends and suppresses Top1-induced mutagenesis at
461 genomic rNMP sites. *Nat Struct Mol Biol* **26**, 155-163, doi:10.1038/s41594-019-0186-1
462 (2019).
463 46 Potenski, C. J., Niu, H., Sung, P. & Klein, H. L. Avoidance of ribonucleotide-induced mutations
464 by RNase H2 and Srs2-Exo1 mechanisms. *Nature* **511**, 251-254 (2014).
465 47 Riva, V. *et al.* Novel alternative ribonucleotide excision repair pathways in human cells by
466 DDX3X and specialized DNA polymerases. *Nucleic Acids Res* **48**, 11551-11565,
467 doi:10.1093/nar/gkaa948 (2020).

468 48 Davies, H. *et al.* HRDetect is a predictor of BRCA1 and BRCA2 deficiency based on mutational
469 signatures. *Nat Med* **23**, 517-525, doi:10.1038/nm.4292 (2017).
470 49 Wang, C. *et al.* Genome-wide CRISPR screens reveal synthetic lethality of RNASEH2
471 deficiency and ATR inhibition. *Oncogene* **38**, 2451-2463, doi:10.1038/s41388-018-0606-4
472 (2019).
473 50 Consortium, T. I. T. P.-C. A. o. W. G. Pan-cancer analysis of whole genomes. *Nature* **578**, 82-
474 93, doi:10.1038/s41586-020-1969-6 (2020).
475

476 **Figure legends**

477 **Fig. 1 | Top1-dependent deletions in *S. cerevisiae* resemble ID4, a cancer mutational signature of**
478 **unknown aetiology. a**, The ID4 signature comprises small deletions (typically 2, 3 or 4 bp in size) of
479 one repeat unit at short tandem repeat (SSTR) and microhomology (MH) sites. i-vi; repeated
480 sequence in bold colour; deletions in red; SNMH, single nucleotide MH. **b**, Indel mutations similar to
481 those detected in ID4 accumulate genome-wide in yeast with high levels of genome-embedded
482 ribonucleotides. Reanalysis of WGS for *rnh201Δ pol2-M644G* yeast²⁵. **c**, Schematic of novel
483 frameshift mutation reporter containing many 2 bp SSTRs. Frameshift mutations in HygroR result in
484 neomycin resistant yeast colonies. P_{TEF}, TEF promoter; HygroR/NeoR, hygromycin/neomycin
485 resistance genes; P2A, self-cleaving peptide. **d,e**, Fluctuation assays demonstrate that Top1-
486 mediated 2 bp SSTR mutations occur in wild-type and RNase H2 deficient (*rnh201Δ*) backgrounds.
487 Mutation rates, median ± 95% confidence intervals for *n*=16 independent cultures per strain (**d**). WT
488 and *rnh201Δ* have similar indel mutation spectra, and differ from *top1Δ* strains. Spectra of neomycin
489 resistant colonies. *n*, number of independent indels detected (**e**). Cosine similarity P-values
490 empirically determined, [Extended Data Fig. 2e,f](#).

491

492 **Fig. 2 | Two bp SSTR deletions are increased in RNase H2 null HeLa cells. a**, Schematic of reporter
493 targeting to AAVS1 safe harbour locus to generate reporter cells. PuroR, puromycin resistance; P_{CAG},
494 CAG promoter; HA, homology arm (L, left; R, right). Also see [Extended Data Fig. 3](#). **b,c**, Validation of
495 *RNASEH2A* knockout reporter clones. Immunoblot of cell lysates detecting the three RNase H2
496 subunits. GAPDH, loading control. For gel source data, see [Supplementary Fig. 1 \(b\)](#). Cellular RNase

497 H2 enzyme activity. Bars, mean; error bars, s.d.; $n=3$ technical replicates. HeLa, no modification;
498 Parental, HeLa with reporter (grey); RNASEH2A+, CRISPR-edited reporter clone retaining RNase H2
499 activity (green); KO1, KO2, CRISPR-mediated *RNASEH2A* knockout clones (red) (c). d, Fluctuation
500 assays establish a significantly increased mutation rate in RNase H2 null (KO) cells. Median \pm 95%
501 confidence intervals. Data points, rates for independent cultures (RNase H2 proficient, RNASEH2A+,
502 $n=9$; knockout, KO1, open circles, $n=10$; KO2, open squares, $n=6$). e, 2 bp SSTR and SNMH deletions
503 are frequent in both RNASEH2A+ and KO cells. Indel mutation spectra. n, number of indels identified
504 by sequencing colonies from independent cultures.

505

506 **Fig. 3 | ID4 SSTR and MH mutations are increased genome-wide in RNase H2 deficient RPE1 cells.**

507 a, Schematic of mutation accumulation experiment. Long-term culture of hTERT-RPE1 *TP53*^{-/-} RNase
508 H2 wildtype (WT) and null cell lines (AKO, BKO: RNASEH2A, RNASEH2B knockout respectively)
509 bottlenecked every 25 doublings by single cell sorting. b, Mutations acquired during long-term
510 culture were significantly enriched for 2-5 bp deletions in RNase H2 null cells, but not other mutation
511 categories (also see [Extended Data Fig 4e](#)). Mean \pm s.d.; P-value, two-sided Fisher's exact test with
512 Bonferroni correction, WT ($n=3$ independent clones) vs KO ($n=2$ independent clones) for 2-5 bp
513 deletions vs all other indel types. c,d, ID4 occurs in RNase H2 null cells (c), and is the major signature
514 once background mutations observed in wildtype cells are subtracted (d).

515

516 **Fig. 4 | RER-deficient tumours have an ID4 signature, associated with transcription and a TNT**

517 **sequence motif.** a, ID4 contributes substantially to the mutational spectrum of Rnaseh2b-KO murine
518 intestinal tumours (WGS, paired tumour-normal samples from $n=6$ mice). b, ID4 contribution is
519 greater in transcribed regions of the genome. Two-sided Fisher's exact test, ID4 vs other indels.
520 $n=969$ indels from 6 biologically independent tumours. c, 2 bp STR/SNMH deletions have biased
521 sequence composition. Genome, frequency of dinucleotides in STR/SNMH sequences in the

522 mappable genome. Deletions (bold red), right aligned. **d,e**, A TNT sequence motif is present at all 2
523 bp STR and SNMH deletions. Sequence logo: Two-bit representation of the sequence context of 2 bp
524 deletions at STR and SNMH sequences (**d**). Deletion sites are significantly enriched for the TNT
525 sequence motif compared to genome-wide occurrence, for all genome sequence, as well as STR and
526 SNMH sites. P-values, Two-sided Fisher's exact test, observed vs expected. $n=228$ (all; $P=1.7 \times 10^{-28}$),
527 124 (STR; $P=0.0008$), 77 (SNMH; $P=1.4 \times 10^{-8}$) deletions in 6 biologically independent tumours (**e**). **f**,
528 Model for TOP1-mediated mutations at TNT sequences containing embedded ribonucleotides, in
529 which strand realignment results in 2 nt deletion (description in main text).

530

531 **Fig. 5 | TOP1-mediated deletions in human cancer and germline.** **a**, 2-5 bp deletions are
532 significantly increased in CLL with biallelic *RNASEH2B* deletions (null). Box, 25-75%; line, median;
533 whiskers 5-95%; data points, values outside range. WT, $n=116$, 85; het (heterozygous), $n=72$, 59; null,
534 $n=10$, 6 tumours (GEL, ICGC respectively). Multiple-testing corrected q-values, 2-sided Mann-
535 Whitney. **b-d**, ID-TOP1 deletions are frequent somatic mutations in cancer. Indels per expression
536 stratum of ubiquitously expressed genes (defined in [Extended Data Fig. 8e](#)). Dotted line, genome-
537 wide rate (**b**). Two bp deletions preferentially occur at TNT motifs. P-values, two-sided Fisher's exact
538 test, observed vs expected. $n=11,853$ (all; $P < 10^{-200}$), 6,699 (STR; $P=1.9 \times 10^{-60}$), 2,872 (SNMH; $P=1.5 \times 10^{-$
539 51) deletions (**c**). 2-5 bp deletions increase with TOP1 cleavage activity in ID4-positive PCAWG
540 tumours (**d**). Solid lines, relative deletion rate. Shading, 95% confidence intervals from 100 (**b**) or
541 1,000 bootstrap replicates (**d**), $n=11,853$ biologically independent tumours⁵⁰ (**b-d**). **e**, 2-5 bp
542 deletions are enriched at tissue-specific highly transcribed genes in associated cancers. Heatmap of
543 significant Odds Ratio scores (2-5 bp deletions in top 10% tissue-restricted genes vs deletions in
544 other genes, relative to expected frequency from all other tissues) for tissue-tumour pairs. Two-
545 sided Fisher's exact test. **f-h**, ID-TOP1 deletions are frequent human *de novo* mutations enriched in
546 highly transcribed germ cell genes. 2-5 bp deletions are the most common indels in the human

547 germline. Gene4Denovo WGS data (³⁹; $n=40,936$ indels) (f). TNT sequence motif is significantly
548 enriched in *de novo* 2 bp deletions (g). P-values, two-sided Fisher's exact test, observed vs expected;
549 $n=5,569$ two bp deletions ($P<10^{-200}$), at STR ($n=3,294$; $P=5.2\times 10^{-47}$) and SNMH sequences ($n=1,093$;
550 $P=2.9\times 10^{-26}$). 2-5 bp deletion frequency correlates with gene transcription level in germ cells (h).
551 Solid lines, Gene4Denovo indel mutations per individual per Mbp. Shading, 95% confidence intervals,
552 100 bootstrap replicates.

553

554 **Methods**

555 **Plasmids**

556 A description of all plasmids used in this work can be found in Supplementary Table 1. The *S.*
557 *cerevisiae* reporter was generated by DNA synthesis (GeneArt Gene Synthesis, Thermo Fisher
558 Scientific; gBlocks Gene Fragments, IDT) and conventional cloning (restriction, ligation and
559 Quikchange site-directed mutagenesis). The final construct (pTCW12) was used for *S. cerevisiae*
560 reporter strain construction and fluctuation assays. A Gateway compatible reporter construct for
561 mammalian cells (pTCW14) was similarly generated using a combination of DNA synthesis and
562 conventional cloning strategies. Gateway cloning was then used to move the reporter cassette into
563 pAAVS-Nst-CAG-Dest (a gift from Knut Woltjen; Addgene plasmid # 80489; ⁵¹) to generate pTCW15
564 for targeting it to the human AAVS1 locus.

565

566 ***In silico* re-design of the Hygromycin resistance gene**

567 To increase the frequency of 2-bp tandem repeats, synonymous substitutions were introduced in the
568 1 kbp *hph* coding sequence, the *Klebsiella pneumoniae* hygromycin resistance gene (HygroR)⁵². Using
569 Python, a 5-codon (15-base) sliding window was moved one codon at a time, to identify all possible
570 synonymous permutations. Permutations were ranked on the basis of tandem dinucleotide repeat

571 sequence length, with the highest ranking sequences used to replace whole codons, prioritising
572 dinucleotide couplet repeats over mononucleotide repeats. Edited codons were then censored from
573 subsequent permutation. Subsequently, to eliminate stop codons that would arise after a 2 bp
574 deletion or equivalent frameshift mutations, further synonymous changes were made, where
575 possible preserving tandem repeat sequences.

576

577 **Yeast strains and growth conditions**

578 All *S. cerevisiae* strains used in this work (Supplementary Table 2) are isogenic with BY4741⁵³ and
579 were grown at 30°C. *TOP1* and *RNH201* open reading frames (ORFs) were deleted using 1-step allele
580 replacement using PCR products generated from plasmid templates with selection cassettes
581 (Supplementary Table 2) and primers containing 60 nt homology directly up and downstream of the
582 ORF. Gene deletions were confirmed by PCR. The 2 bp deletion reporter was inserted at the *AGP1*
583 locus using a PCR product amplified from pTCW12 using primers AGP1-MX6-F and AGP1-MX6-R
584 (Supplementary Table 3). Correct reporter insertion was confirmed by PCR and Sanger sequencing.
585 Growth under selection was on YPD (10 g/l yeast extract, 20 g/l bactopectone, 20 g/l dextrose, 20 g/l
586 agar) supplemented with hygromycin B (300 mg/l), nourseothricin (100 mg/l) and/or G418 (1 g/l), or
587 on Synthetic Defined medium (6.7 g/l yeast nitrogen base without amino acids, complete
588 supplement single dropout mixture (Formedium), 20 g/l dextrose, 20 g/l agar).

589

590 **Fluctuation assays (yeast)**

591 Fluctuation assays were performed as previously described⁵⁴. Yeast was grown overnight in YPD with
592 hygromycin B (300 mg/l), plated on YPD and grown at 30°C to obtain individual colonies derived
593 from a single cell without HygroR mutations. For each strain, 16 independent colonies were then
594 used to inoculate 5 ml YPD, and grown for 3 days at 30°C with shaking at 250 rpm. Cells were

595 pelleted by centrifugation and resuspended in 1 ml of H₂O. Undiluted suspensions for each culture
596 were plated (100 µl per plate) on 2 YPD plates supplemented with 1 g/l G418, with the exception of
597 *rnh201Δ* for which a 10⁻² dilution was used. In addition, each suspension was serially diluted to 10⁻⁶
598 of which 100 µl per plate was spread on 2 YPD plates to estimate the total number of viable cells per
599 culture. Plates were incubated at 30°C for 2-3 days, and colonies counted. Mutation rates were
600 determined in Microsoft Excel 2016 for each individual culture, and an overall rate for each strain
601 calculated using the Lea Coulson method of the median⁵⁵. The number of mutants for each culture
602 were ranked, and those ranked 4rd and 13th used to calculate the rates that define the lower and
603 upper limits of the 95% confidence interval⁵⁶. A single G418-resistant colony for each independent
604 culture was used to determine the spectrum of frame shift mutations. A 1.3 kbp region including
605 HygroR was amplified in two overlapping amplicons (primers S297F and S1113R; S752 and S1658R)
606 using FastStart PCR Master Mix (Roche) and direct colony PCR (5 min 95°C; 35 cycles 30 s 95°C, 30 s
607 58°C, 45 s 72°C; 45 s 72°C). Each amplicon was Sanger sequenced using primers described in
608 Supplementary Table 3, and analysed using Sequencher 5.4.6 (Gene Codes Corporation) and/or
609 Mutation Surveyor V3.30 (SoftGenetics). Mutation rates (per bp) were calculated for 1,032 bp of
610 sequence in which productive frameshift mutations can occur.

611

612 **Cell lines**

613 Human cell lines used in this work are summarised in Supplementary Table 4. All cells were grown at
614 37°C and 5% CO₂, authenticated using STR DNA profiling in the labs of origin and shown to be
615 mycoplasma negative through routine testing. HeLa cells (a gift from G. Stewart, University of
616 Birmingham, UK; originally purchased from ATCC) were grown in Dulbecco's Modified Eagle Medium
617 (DMEM; Gibco/Thermo Fisher Scientific) supplemented with 10% fetal bovine serum (FBS), 100 U/ml
618 penicillin and 100 µg/ml streptomycin. hTERT-RPE1 cells (a gift from D. Durocher, University of
619 Toronto, Canada; originally purchased from ATCC) were grown in DMEM/F12 medium mixture

620 (Gibco/Thermo Fisher Scientific) supplemented with 10% FBS, 100 U/ml penicillin and 100 µg/ml
621 streptomycin. The 2-bp deletion reporter was integrated at the *AAVS1* safe harbour locus in HeLa
622 cells using a published CRISPR/Cas9 targeting protocol⁵¹. HeLa cells were transfected with pXAT2
623 and pTCW15 in Opti-MEM reduced-serum medium using Invitrogen Lipofectamine 2000 (Thermo
624 Fisher Scientific). After 48 h cells were re-plated in medium containing 500 µg/ml G418, and after
625 another 48 h and a second round of re-plating in selective medium, single cells were sorted into 96-
626 well plates using a BD FACSJazz instrument (BD Biosciences). Resulting G418-resistant clones were
627 screened by PCR for reporter integration at the correct locus, retention of integration-free *AAVS1*
628 and Sanger sequencing of resulting PCR products. Single-locus integration was confirmed by FISH as
629 previously described⁵⁷, using pTCW16 to generate a fluorescently labelled probe. The full reporter
630 sequence of selected clones was checked, with amplification of a 1.9 kbp fragment using Prime Star
631 Max PCR Master Mix (Takara Bio) with primers HygroR_up and PuroR_rev (40 cycles 10 s 98°C, 15 s
632 70°C, 2 min 72°C), followed by Sanger sequencing with additional primers (Supplementary Table 3).
633 To generate RNASEH2A-KO reporter cells, the selected parental HeLa reporter clone was transfected
634 with pMAR526 and pMAR527 (Supplementary Table 1), using Lipofectamine 2000. Forty-eight hours
635 after transfection, single EGFP-expressing cells were sorted into 96-well plates and grown until
636 colonies formed. Initial screening was based on PCR amplification (primers RNASEH2A-ex1F and
637 RNASEH2A-ex1R) of the CRISPR/Cas9-targeted region of *RNASEH2A* with mutations present in
638 selected clones determined by Sanger sequencing. The cellular RNase H2 status was then confirmed
639 by immunoblotting, RNase H2 enzymatic activity assay, and alkaline gel electrophoresis to determine
640 ribonucleotide content of genomic DNA (detailed methods below).

641

642 **Fluctuation assays (human)**

643 Hygromycin resistant HeLa reporter cells (400 µg/ml hygromycin B) were recovered from frozen
644 stocks in the absence of selection. The following day, 10 wells of a 96-well plate were seeded with

645 2,000 cells per well for each line. The experiment was performed with the operator blinded to the
646 identity of the cell lines. Cells were cultured under non-selective conditions and re-plated
647 subsequently in 24-well, 6-well plates and ultimately T75 flasks, in which they were grown to
648 confluence. Cells were then dissociated using Gibco TrypLE (Thermo Fisher Scientific) and cells
649 counted using a Moxi Z automated cell counter. After serial dilution 1,000 cells were plated into two
650 10-cm plates for each culture and grown for 14 days to determine plating efficiency. All other cells
651 were plated into two 10-cm plates, 0.5 µg/ml puromycin added after 4 h, with medium subsequently
652 changed every 2-3 days for 14 days to remove dead cells and maintain a puromycin concentration of
653 0.5 µg/ml.

654 To establish mutation spectra, colonies were removed by scraping and then cultured in a 96-well
655 plate. When confluent, cells were lysed with 75 µl DirectPCR Lysis Reagent (Viagen Biotech) and 0.4
656 mg/ml PCR-grade Proteinase K (Roche), heating overnight at 55 °C followed by 45 min at 85 °C. Only
657 one sample per independent culture was used for PCR amplification and Sanger sequencing to
658 determine the nature of mutations in the HygroR coding sequence. A 1.24 kbp region including
659 HygroR was amplified with Prime Star Max PCR Master Mix (Takara Bio), HygroR_up and H1327R
660 primers (40 cycles 10 s 98°C, 15 s 70°C, 2 min 72°C). Sanger sequencing was then performed with
661 additional primers (Supplementary Table 3) and mutations identified using Mutation Surveyor V3.30
662 (SoftGenetics). All mutants showed double traces of equal height from the point of indel mutations,
663 consistent with the presence of two copies of the reporter in all reporter lines. As FISH indicated
664 presence of the reporter at a single AAVS1 locus, we inferred that two copies of the reporter were
665 inserted in tandem at this locus. As a 2 bp deletion or equivalent frameshift mutation in either
666 HygroR copy would bring the associated PuroR coding sequence into the translated reading frame,
667 we corrected mutation rate calculations (per bp) for the presence of 2 copies.

668 To determine colony numbers, plates were washed with PBS, fixed with 2% formaldehyde in PBS for
669 10 min, rinsed with water, and colonies stained with 0.1% crystal violet solution for 10 min. Plates

670 were then washed with water and left to dry before counting colonies. After counting the
671 experiment was unblinded. Mutation rates were determined for each individual culture in Microsoft
672 Excel 2016, and an overall rate for WT and KO strains calculated using the Lea Coulson method of
673 the median. The number of mutants for each culture were ranked, and appropriate ranks⁵⁶ used to
674 calculate the rates that define the lower and upper limits of the 95% confidence interval.

675

676 **Immunoblotting**

677 Whole-cell extracts (WCE) to determine protein levels of RNase H2 subunits by immunoblotting and
678 for RNase H2 activity assays were prepared as previously described⁵⁸. Equal amounts of protein from
679 WCE were separated by SDS-PAGE on 4-12% NuPAGE gels and transferred to PVDF. Membranes
680 were probed in 5% milk (w/v; Marvel Original Dried Skimmed), TBS+0.2% Tween-20 (v/v) with the
681 following antibodies: sheep anti-RNase H2 (raised against human recombinant RNase H2, 1:1,000)¹⁴;
682 mouse anti-RNASEH2A G-10 (Santa Cruz Biotechnologies sc-515475, lot #A1416, 1:1,000); rabbit
683 anti-GAPDH (Abcam ab9485, 1:2,000, lot #GR3380498-1). For detection we Rabbit Anti-Sheep
684 Immunoglobulins/HRP (Dako, P04163, lot #00047199, 1:2,000); Goat Anti-Mouse
685 Immunoglobulins/HRP (Dako, P0447, lot #20039214, 1:10,000); Anti-rabbit IgG, HRP-linked Antibody
686 (Cell Signaling Technologies, 7074S, lot #29, 1:10,000); Amersham ECL Prime Western Blotting
687 Detection Reagent (GE Healthcare Life Sciences) and an ImageQuantLAS4000 device, or IRDye
688 secondary antibodies and an Odyssey CLx Imaging System (LI-COR Biosciences). Uncropped
689 immunoblots are presented in Supplementary Fig. 1.

690

691 **RNase H2 activity assays**

692 To assess cellular RNase H2 activity, a FRET-based fluorescent substrate release assay was
693 performed as previously described¹⁴. Briefly, RNase H2-specific activity was determined by

694 measuring the cleavage of double-stranded DNA substrate containing a single embedded
695 ribonucleotide. Activity against a DNA-only substrate of the same sequence was used to correct for
696 background activity. Substrates were formed by annealing a 3'-fluorescein-labeled oligonucleotide
697 (GATCTGAGCCTGGGgGCT or GATCTGAGCCTGGGAGCT; uppercase DNA, lowercase RNA) to a
698 complementary 5'-DABCYL-labelled DNA oligonucleotide (Eurogentec). Reactions were performed in
699 100 µl reaction buffer (60 mM KCl, 50 mM Tris-HCl pH 8.0, 10 mM MgCl₂, 0.01% BSA, 0.01% Triton
700 X-100) with 250 nM substrate in black 96-well flat-bottomed plates (Costar) at 24°C. WCE was
701 prepared as described above, protein concentrations determined using a Bio-Rad Bradford Protein
702 Assay, and the final protein concentration per reaction was 50 ng/µl. Fluorescence was read (100
703 ms) every 5 min for up to 90 min using a VICTOR2 1420 multilabel counter (Perkin Elmer), with a
704 480-nm excitation filter and a 535-nm emission filter. Initial substrate conversion after background
705 subtraction was used to calculate RNase H2 enzyme activity.

706

707 **Alkaline gel electrophoresis**

708 To determine the presence of excess genome-embedded ribonucleotides in nuclear DNA, alkaline
709 gel electrophoresis of RNase H2 treated genomic DNA was performed as previously described⁵⁸.
710 Briefly, total nucleic acids were isolated from pellets from ~1 million cells by incubation in ice-cold
711 buffer (20 mM Tris-HCl pH 7.5, 75 mM NaCl, 50 mM EDTA) with 200 µg/ml proteinase K (Roche) for
712 10 min on ice, followed by addition of N-lauroylsarcosine sodium salt (Sigma) to a final concentration
713 of 1%. Nucleic acids were phenol:chloroform-extracted, isopropanol precipitated and dissolved in
714 nuclease-free water. For alkaline gel electrophoresis, 500 ng of total nucleic acids was incubated
715 with 1 pmol of purified recombinant human RNase H2 (isolated as previously described⁵⁹) and 0.25
716 µg of DNase-free RNase (Roche) for 30 min at 37°C in 100 µl reaction buffer (60 mM KCl, 50 mM
717 Tris-HCl pH 8.0, 10 mM MgCl₂, 0.01% Triton X-100). Nucleic acids were ethanol precipitated,
718 dissolved in nuclease-free water and 250 ng separated on 0.7% agarose gels in 50 mM NaOH, 1 mM

719 EDTA. After overnight electrophoresis, the gel was neutralised in 0.7 M Tris–HCl pH 8.0, 1.5 M NaCl
720 and stained with SYBR Gold (Invitrogen). Imaging was performed on a FLA-5100 imaging system
721 (Fujifilm), and densitometry plots were generated using AIDA Image Analyzer v3.44.035 (Raytest).

722

723 **Mutation accumulation experiment**

724 TP53-KO hTERT-RPE1 cells without and with loss-of-function mutations in *RNASEH2A* or *RNASEH2B*,
725 introduced by CRISPR/Cas9 genome editing, a gift from D. Durocher (The Lunenfeld–Tanenbaum
726 Research Institute, Toronto), have been previously described³³. RNase H2 proficient (WT),
727 *RNASEH2A*-KO and *RNASEH2B*-KO cells were single cell sorted into 96-well plates using a BD
728 FACSJazz instrument (BD Biosciences). Multiple individual clones for each were expanded to
729 confluent T75 flasks for cryopreservation and genomic DNA isolation of these ancestral populations.
730 In addition, lines were again single cell sorted into 96-well plates to start the mutation accumulation
731 experiment. Cultures were expanded by subsequent growth in 24-well, 6-well plates and T75 flasks
732 until confluent (approximately 25 population doublings), and this process of single cell sorting and
733 expansion was repeated 4 more times providing bottlenecks to capture mutations that occurred
734 since the previous sort. From the first to the last single cell sort a total of approximately 100
735 population doublings occurred and the final culture was expanded for cryopreservation and genomic
736 DNA isolation of these end-point populations.

737 Genomic DNA was isolated using phenol extraction as previously described⁵⁸, for alkaline gel
738 electrophoresis and whole genome sequencing. Library preparations and sequencing were
739 performed by Edinburgh Genomics. Libraries were prepared using Illumina SeqLab specific TruSeq
740 PCRFree High Throughput library preparation kits as per manufacturer's instructions, with DNA
741 samples sheared to a 450 bp mean insert size. Libraries were sequenced using paired-end reads on
742 an Illumina HiSeqX instrument using v2.5 chemistry to achieve minimum mean genome-wide
743 sequencing depth of 30x per sample.

744

745 **Mouse whole genome sequencing**

746 Villin-Cre⁺ Trp53^{fl/fl} Rnaseh2b^{fl/fl} mice with epithelial-specific deletion of *Trp53* and *Rnaseh2b* on a
747 C57Bl/6J background have been described previously²⁹. Animal experiments were conducted with
748 appropriate permission, in accordance with guidelines for animal care of the Christian-Albrechts-
749 University (Kiel, Germany), in agreement with national and international laws and policies. No
750 randomisation or blinding was performed. Paired tumour-normal DNA was isolated from small
751 intestinal tumours (*Trp53*^{-/-} *Rnaseh2b*^{-/-}) and liver tissue (*Trp53*^{+/+} *Rnaseh2b*^{+/+}) from 52-week old
752 females, using a Qiagen DNeasy Blood & Tissue Kit. Library preparations and sequencing were
753 performed by Edinburgh Genomics using Illumina DNA PCR-Free Library Prep as per manufacturer's
754 instructions. Paired end sequencing was performed by Edinburgh Genomics on a NovaSeq 6000
755 using v1.5 chemistry. Mean genome-wide sequencing depth of at least 30x for liver samples and 60x
756 for tumour samples was obtained.

757

758 ***S. cerevisiae* WGS analysis**

759 Whole genome sequencing SRA files for *rnh201Δ pol2-M644G S. cerevisiae*²⁵ from the NCBI
760 Sequence read archive (SRA) were converted to FASTQ files using SRA Toolkit v2.5.4-1 (SRA Toolkit
761 Development Team; <http://ncbi.github.io/sra-tools/>). FASTQ reads were aligned to the
762 GSE56939_L03_ref_v2 reference genome (⁶⁰; Supplementary Table 5) and sorted BAM files created
763 using BWA-MEM 0.7.12⁶¹, and deduplicated with SAMBLASTER v0.1.22⁶². To select high quality indel
764 variants, GATK (v3.6-0) Haplotype Caller (without Base Quality Score Recalibration)⁶³ variant calling
765 was performed with "Hard Filters" (--filterExpression "QD < 2.0 || FS > 200.0 || ReadPosRankSum < -
766 20.0"). Filtering for strain-specific variants was performed as previously described⁶⁰, with minor
767 modifications. Filters: 1) eliminate variants shared with an ancestral clone; 2) required ≥ 20 reads for

768 variant allele in descendent; 3) exclusion of repetitive sequences as defined in ⁶⁰; 4)
769 reference/variant depth ratio 0.4-0.6; < 0.4 if homozygous variant allele .

770

771 **RPE1 WGS analysis**

772 FASTQs were converted to unaligned BAM format and Illumina adaptors marked using GATK v4.1.9.0
773 FastqToSam and MarkIlluminaAdapters tools⁶⁴. Reads were aligned to the human genome (hg38,
774 including alt, decoy and HLA sequences) using BWA-MEM v0.7.16 ⁶¹ and read metadata merged
775 using GATK's MergeBamAlignment tool. PCR and optical duplicate marking and base quality score
776 recalibration were performed using GATK. Variants from NCBI dbSNP build 151 were used as known
777 sites for base quality score recalibration. Post-processed alignments were genotyped using Mutect2,
778 Strelka2, Platypus and SvABA using somatic calling models for each pair of ancestral and endpoint
779 cultures, as detailed below.

780

781 **Mouse WGS analysis**

782 FASTQ processing and alignment was performed as for RPE1 WGS analysis, using the GRCm38 mouse
783 genome reference and known variant sites from the Mouse Genomes Project⁶⁵ (REL-1807-
784 SNPs_Indels) for base quality score recalibration. Somatic variant calling of post-processed
785 alignments was performed using Mutect2, Strelka2, Platypus and SvABA for each tumour-liver pair,
786 as detailed below. Somalier v0.2.12 (<https://github.com/brentp/somalier>) was used to confirm each
787 paired tumour and liver sample originated from the same animal.

788

789 **Human Ethics approval**

790 Data generated from Genomics England 100,000 genomes and ICGC-CLL studies were analysed. In
791 these respective studies, informed consent for participation was obtained. Ethical approval for
792 Genomics England 100,000 genomes project: East of England and South Cambridge Research Ethics
793 Committee; CLL-ICGC: International Cancer Genome Consortium (ICGC) guidelines from the ICGC
794 Ethics and Policy committee were followed and the study was approved by the Research Ethics
795 Committee of the Hospital Clínic of Barcelona.

796

797 **CLL WGS analysis**

798 *Genomics England*: CLL tumour-normal pairs ($n=198$) were processed as part of the 100,000
799 Genomes Project (pilot and main programme v8). Samples were sequenced using the Illumina HiSeq
800 X System with 150 bp paired-end reads at a minimum of 75x coverage for tumours and 30x coverage
801 for germline samples. Reads were mapped to GRCh38 using ISAAC aligner v03.16.02.19⁶⁶. SNVs and
802 indels were called using Strelka v2.4.7 using somatic calling mode. Structural and copy number
803 variants were called using Manta v0.28.0 and Canvas v1.3.1⁶⁷, respectively. Samples with a tumour
804 purity estimate from Canvas of less than 50% were excluded from analysis. *RNASEH2B* copy number
805 was determined using a combination of Canvas, Manta, read depth counts with samtools v1.9 and
806 confirmed by manual inspection using IGV (v2.5.0)⁶⁸.

807 *ICGC*: WGS from the ICGC-CLL cohort³⁵ ($n=150$) was re-analysed. Raw reads were mapped to the
808 human reference genome (GRCh37) using BWA-MEM (v0.7.15)⁶¹. BAM files were generated, sorted,
809 indexed and optical or PCR duplicates flagged using biobambam2
810 (<https://gitlab.com/german.tischler/biobambam2>, v2.0.65). Copy number alterations were called
811 from WGS data using Battenberg (cgpBattenberg, v3.2.2)⁶⁹, ASCAT (ascatNgs, v4.1.0)⁷⁰, and Genome-
812 wide Human SNP Array 6.0 (Thermo Fisher Scientific) data³⁵ re-analysed using Nexus 9.0
813 Biodiscovery software (Biodiscovery). *RNASEH2B* copy number was established by combining the
814 three analyses and manual review with IGV.

815

816 **Colorectal Cancer WGS analysis**

817 Irinotecan-treated ($n=39$) and irinotecan-untreated ($n=78$) colorectal cancers from the 100,000
818 Genomes Project Colorectal Cancer Domain were 1:2 matched using a multivariate greedy matching
819 algorithm without replacement, implemented in the Matching R-package⁷¹. Matching was
820 conducted considering sex, age at sampling, whether a primary tumour or metastasis had been
821 sequenced, microsatellite instability status, and whether the individual have previously received
822 radiotherapy, oxaliplatin, capecitabine or fluorouracil treatment.

823

824 **Somatic Variant Calling**

825 Somatic variant calling was performed in parallel using four distinct methods: Mutect2 (as part of
826 GATK v4.1.9.0)^{72,73}, Strelka2 (v2.1.9.10)⁷⁴, SvABA (v1.1.3)⁷⁵ and Platypus (v0.8.1)⁷⁶. High-confidence
827 indel calls were defined as the intersected output of these four tools, where variants passed all
828 filters for ≥ 3 of 4 callers. The intersection was performed using the bcftools (v1.10.2)⁷⁷ isec function
829 after normalising variant calls and left-aligning ambiguous alignment gaps using the bcftools norm
830 function. For Platypus (v0.8.1)⁷⁶, joint calling all samples in each cohort was performed before
831 filtering for somatic variants; the other variant callers were run in paired tumour-normal mode. For
832 the RPE1 mutation accumulation experiment the endpoint and ancestral cultures were defined as
833 “tumour” and “normal” samples respectively. Variant filtering strategies were optimised to both
834 available information on segregating genetic variation for humans and mice, and the functionality of
835 each calling method as detailed below.

836 *Mutect2*: unfiltered genotypes for all normal samples were combined to filter germline variants.

837 Somatic calls were obtained using GATK’s FilterMutectCalls command. Human polymorphism data

838 and allele frequencies from, gnomAD⁷⁸ were provided to Mutect2 for the filtering of germline
839 variants.

840 SvABA: Germline indel and structural variants were filtered using --dbsnp-vcf and --germline-sv-
841 database options. Mouse indels were obtained from Mouse Genomes Project version 5 SNP and
842 ([ftp://ftp-mouse.sanger.ac.uk/REL-1505-](ftp://ftp-mouse.sanger.ac.uk/REL-1505-SNPs_Indels/mgp.v5.merged.indels.dbSNP142.normed.vcf.gz)
843 [SNPs_Indels/mgp.v5.merged.indels.dbSNP142.normed.vcf.gz](ftp://ftp-mouse.sanger.ac.uk/REL-1505-SNPs_Indels/mgp.v5.merged.indels.dbSNP142.normed.vcf.gz)); structural variants from SV release
844 version 5 (ftp://ftp-mouse.sanger.ac.uk/REL-1606-SV/mgpv5.SV_insertions.bed.gz and [ftp://ftp-](ftp://ftp-mouse.sanger.ac.uk/REL-1606-SV/mgpv5.SV_deletions.bed.gz)
845 [mouse.sanger.ac.uk/REL-1606-SV/mgpv5.SV_deletions.bed.gz](ftp://ftp-mouse.sanger.ac.uk/REL-1606-SV/mgpv5.SV_deletions.bed.gz)). Human indels were extracted from
846 NCBI dbSNP build 151 and common structural variants from dbVAR
847 (<https://hgdownload.soe.ucsc.edu/gbdb/hg38/bbi/dbVar/>).

848 Strelka2: candidate small indels for each pair were first generated by Manta (v1.6.0)⁷⁹ in somatic
849 calling mode. Strelka2 was then executed in somatic calling mode for each pair with Manta's
850 candidate small indels output provided to the --indelCandidates option.

851 Platypus: Germline variants were filtered on the basis of any "normal" sample with ≥ 2 variant allele
852 reads. Somatic variant calls for each sample pair were retained if "tumour"/endpoint sample > 2
853 variant reads; site depth > 9 ; and "normal" sample read depth ≥ 20 , < 2 variant reads. Additionally, a
854 $> 10x$ ratio of tumour to normal for variant/total depth was required.

855 For Genomics England CLL tumour-normal pairs, pre-existing Strelka2 calls from the 100,000
856 Genomes Project pipeline were used, while variant calling with Mutect2, Platypus and SvABA was
857 performed as above. Colorectal cancer tumour-normal pairs from Genomics England were processed
858 as for Genomics England CLL but without Mutect2 analysis. For ICGC CLL, somatic indels were called
859 using Mutect2 (GATK v4.0.2.0)^{72,73}, Strelka2 (v2.8.2)⁷⁴, SvABA (v1.1.0)⁷⁵, and Platypus (v0.8.1)⁷⁶.

860 Candidate small indels generated by Manta (v1.2)⁷⁹ were used as input for Strelka2. Mutect2,
861 Strelka2 and SvABA were run in paired tumour-normal mode. somaticMutationDetector.py
862 (<https://github.com/andyrimmer/Platypus/tree/master/extensions/Cancer>) was used to identify

863 somatic indels called by Platypus with a minimum posterior of 1. SNVs called by Platypus were
864 considered somatic if they had at least 2 alternative reads in the tumour, fewer than 2 alternative
865 reads in the normal, a minimum tumour VAF of 10x the control VAF, and a minimum depth of 10.

866

867 **Germline mutation analysis**

868 *De novo* WGS variants were downloaded from the Gene4Denovo database (Supplementary Table 5).

869 Reference assembly conversion errors were removed by discarding variants where the reference

870 allele did not match the genome reference at the given position or where the variant position was

871 greater than the length of the reference chromosome. In addition, individuals with total *de novo*

872 variants below the 10th ($n=33$) or above the 90th ($n=140$) percentile were excluded. For germline

873 gene expression we used pre-defined expression groups⁸⁰ based on Ensembl release 90 annotation

874 (ftp://ftp.ensembl.org/pub/release-90/gtf/homo_sapiens/Homo_sapiens.GRCh38.90.gtf.gz). Initially

875 stratified as nine expression groups from 1 (=unexpressed) to 9 (=high), we collapsed them into a

876 smaller set of unexpressed (1), low (2, 3, 4), mid (5, 6, 7) and high (8, 9). The annotations were

877 converted to GRCh37 coordinates using liftover (kent source version 417). Genomic segments

878 overlapping multiple distinct expression groups, due to overlapping genes, were assigned to the

879 higher of those expression groups. For each expression group we summed the count (c) of *de novo*

880 indels contained within the genomic span of those genes. This was converted to rate estimates by

881 dividing by the union genomic span (g nucleotides) of genes in that expression group, and adjusting

882 for the number of mutated genomes considered (n); $rate = c/(gn)$. To obtain 95% confidence

883 intervals, gene selection was bootstrapped (sampled to an identical number with replacement) 100

884 times and the 0.025 and 0.975 quantiles of the bootstrapped rate calculation taken as the 95%

885 confidence interval.

886

887 **ICGC Pan-cancer expression analysis**

888 The ICGC PCAWG somatic mutations⁵⁰
889 (https://dcc.icgc.org/api/v1/download?fn=/PCAWG/consensus_snv_indel/final_consensus_passonly
890 [.snv_mnv_indel.icgc.public.maf.gz](https://dcc.icgc.org/api/v1/download?fn=/PCAWG/consensus_snv_indel/final_consensus_passonly)) and ICGC PCAWG “baseline” gene expression⁵⁰ were obtained
891 (ArrayExpress <https://www.ebi.ac.uk/arrayexpress/experiments/E-MTAB-5200/>). Genomic
892 annotation of gene extents on the GRCh37 reference genome match the Ensembl version 75
893 annotation ([http://ftp.ensembl.org/pub/release-](http://ftp.ensembl.org/pub/release-75/gtf/homo_sapiens/Homo_sapiens.GRCh37.75.gtf.gz)
894 [75/gtf/homo_sapiens/Homo_sapiens.GRCh37.75.gtf.gz](http://ftp.ensembl.org/pub/release-75/gtf/homo_sapiens/Homo_sapiens.GRCh37.75.gtf.gz)) of the ICGC gene expression calls. Mean,
895 median and maximal gene expression (transcripts per million, TPM) were calculated for each gene
896 across the 76 ICGC baseline gene expression tissues/samples. Only genes annotated on the main
897 autosomal chromosomes, 1 to 22 and the X chromosome were considered. Overlapping genes were
898 removed, keeping only the most abundantly (highest median, then mean in the case of ties)
899 expressed genes from overlapping pairs. This filtering was applied hierarchically, starting with the
900 most abundant. Following⁸¹ genes with housekeeping-like expression were defined as those with
901 maximal expression of less than ten times median expression. Housekeeping-like genes were decile
902 binned into expression groups based on median expression. Mutations were stratified by type (1 bp
903 deletion, 2-5 bp deletion) or by the “TN*T” motif defined below and counted by intersection with
904 the annotated genomic extents of genes in each expression group.

905 For the analysis of tissue-biased gene expression, the 76 ICGC baseline samples were grouped by
906 annotated tissue (e.g. breast, prostate, kidney, liver) and matched where possible to the tissue of
907 origin for ICGC cancer types. For each tissue, the median expression (in TPM) of each gene was
908 calculated for (a) within-tissue samples and (b) for all other samples. The 90th quantile of gene
909 expression (q90, top 10%) within a tissue was set as a threshold for “high” level expression. Genes
910 with high expression in a tissue (a) but a median expression of less than $q90 \cdot 0.1$ in the other tissues
911 (b) were considered highly expressed but tissue restricted (HETR). For the set of HETR genes from a
912 tissue, we counted the number of 2-5 bp deletions within the annotated genomic extent of the HETR
913 genes in a cancer type of interest. We similarly counted 2-5 bp deletions in all other genes for that

914 cancer type, and counted both the HETR and non-HETR 2-5 bp deletions from all other cancer types
915 within the ICGC cohort. For each cancer:tissue pair this provided 4 sets of counts, analysed as two-
916 tailed Fisher's exact test using the R `fisher.test` function. A positive odds-ratio indicating enrichment
917 of 2-5 bp deletions in the HETR genes, compared to a background of the remainder of the ICGC
918 cohort in which HETR genes are not highly expressed. For each cancer type considered, this test was
919 repeated for each tissue type ($n=17$). Analyses were carried out for eight of the ICGC cohort cancer
920 types which met the combined criteria of having a well-matched and known tissue of origin amongst
921 the ICGC baseline samples, and requiring the cancer type cohort to have at least $n=2,500$ 2-5 bp
922 deletions in aggregate. This represents $n=17*8=136$ statistical tests, adjusted for by Bonferroni
923 correction. Odds ratios (r) for mutation depletion were transformed to their reciprocal ($1/r$) for
924 display purposes.

925

926 **ICGC Pan-cancer TOP1-seq analysis**

927 Data corresponding to two replicates of TOP1-seq, a modified ChIP-seq technique to
928 immunoprecipitate only catalytically engaged TOP1³⁸, were downloaded from the NCBI GEO
929 database (accession code GSE57628, samples GSM1385717 and GSM1385718). Autosomal
930 chromosomes 1 to 22 and the X chromosome were divided into 1 kbp bins and for each bin the
931 amount of mappable sequence was determined using Umap's regions mappable using 36mers⁸² to
932 approximate read length of the TOP1-seq data. For each 1 kbp window, the TOP1-seq signal within
933 mappable regions was summed for each replicate and mean signal calculated. This mean was
934 divided by the amount of mappable sequence to calculate the TOP1-seq signal per bp and each 1 kb
935 window was then assigned to decile bins using this value.

936 Somatic deletion calls from ID4-positive PCAWG samples (as defined in
937 [https://dcc.icgc.org/api/v1/download?fn=/PCAWG/mutational_signatures/Signatures_in_Samples/S](https://dcc.icgc.org/api/v1/download?fn=/PCAWG/mutational_signatures/Signatures_in_Samples/S_P_Signatures_in_Samples/PCAWG_SigProfiler_ID_signatures_in_samples.csv)
938 [P_Signatures_in_Samples/PCAWG_SigProfiler_ID_signatures_in_samples.csv](https://dcc.icgc.org/api/v1/download?fn=/PCAWG/mutational_signatures/Signatures_in_Samples/S_P_Signatures_in_Samples/PCAWG_SigProfiler_ID_signatures_in_samples.csv)) were counted within

939 the same 36-mer mappable regions for each 1kbp window and either stratified by type (1 bp
940 deletion, 2-5 bp deletion) or by the “TN*T” motif defined below. Relative rates of deletions in each
941 category were calculated relative to the first TOP1-seq signal decile.

942

943 **Mutational signatures**

944 *De novo* extraction and decomposition of mutational signatures was performed in Python 3.8.5 using
945 SigProfilerExtractor (v1.1.0)⁵, along with SigProfilerMatrixGenerator (v1.1.14/1.1.15)⁸³ and
946 SigProfilerPlotting (v1.1.27). Recommended default settings (including 500 NMF replicates) were
947 applied (<https://github.com/AlexandrovLab/SigProfilerExtractor>). Subtraction of mutations in RPE1
948 wildtype cells from those detected in RNase H2 null cells was performed as follows. The average
949 number of indels per line for each of the 83 categories was determined for the three wildtype lines.
950 Counts per category for AKO and BKO lines were subtracted using these averages, with negative
951 values set to 0. SigProfilerExtractor was then performed on the resulting WT-subtracted AKO and
952 BKO ID-83 matrices for both *de novo* signature detection and decomposition analysis.

953

954 **Indel sequence context analysis**

955 WGS indels were categorized based on repeat sequence context. Genome-wide occurrence of short
956 repeats and regions of microhomology were identified and filtered to include only the mappable
957 genome, defined by Umap’s regions mappable using 100mers⁸². For both WGS-identified indel
958 variants and genome-wide occurrence, scoring of 2-bp deletions compliant with the “TNT” motif at
959 MH/SSTR sites required the deleted bases to match the sequence NT with a T immediately 5’ of the
960 deleted dinucleotides. More generally, for varying sized deletions these were considered to fit a
961 “TN*T” motif if the deletion lay within an SSTR or region of microhomology containing the motif $TN_{(d)}$
962 $_{-1}T$ where d = the length of the deletion. Genome-wide occurrences were estimated from 100,000

963 randomly generated deletions of given lengths within the mappable genome. For SSTRs and MH
964 regions, all regions containing the respective motifs $(\text{TN}_{(r-1)})_n$ or $\text{TN}_{(r-1)}\text{T}$ were identified (where $r =$
965 the length of the repeat unit and $n > 1$), and the fraction of SSTR/MH sequence containing TNT
966 motifs determined against total SSTR/MH sequence in the mappable genome.

967 To derive a null expectation for *de novo* deletions matching the TNT, TNNT and TNNNT motif for 2, 3,
968 and 4 bp deletions respectively, deletions at repeats from the Gene4Denovo database were first
969 classified by deletion length, repeat type (STR or MH) and repeat length. Bootstrap samples of
970 corresponding repeats from the genome were generated with 1,000 replicates. That is, for each
971 deletion category an equal number of repeats of matching repeat type, repeat unit length and total
972 repeat length were randomly drawn from the genome for each bootstrap sample.

973

974 **Sequence logos**

975 Genomic sequences containing 2 bp deletions were reversed and complemented when the deleted
976 dinucleotide contained an adenosine (A), except when the dinucleotide was AT or TA. For SNMH and
977 STR deletions, the position of the deleted dinucleotide cannot be unequivocally assigned, and
978 therefore the deleted sequence was right aligned in the repeat/microhomology region, either to the
979 most 3' T, where present, or otherwise to the limit of the repeat/microhomology region. Sequences
980 were converted to bit score matrices and logos drawn using Logomaker v0.8⁸⁴.

981

982 **Embedded ribonucleotide sequence context analysis**

983 EmRiboSeq data from *rnh201Δ* yeast prepared during mid-log phase growth⁸⁵ was obtained
984 (Supplementary Table 5) and aligned to the sacCer3 reference genome as previously described to
985 identify the genomic coordinates of genome embedded ribonucleotides⁸⁶. Bedtools (version v2.30.0,
986 ⁸⁷) utilities groupby, slop and getfasta were used to extract and count the sequence context of

987 genome embedded ribonucleotides with downstream analysis and plotting implemented in R
988 (version 4.0.5). Genome sequence composition adjusted relative rates were calculated as previously
989 described³² such that under the null expectation of no sequence bias in ribonucleotide
990 incorporation, all sequence contexts have an expected relative rate of 1/n where n is the number of
991 contexts considered.

992

993 **Statistical methods**

994 Statistical testing was performed using GraphPad Prism v9.1.1, Python v3.8.5 or R v3.3.1. Two-side
995 non-parametric Mann-Whitney tests were performed for quantitative measurements; multiple
996 testing correction, FDR set at 0.05; and for categorical data Fisher's exact tests were performed in
997 Python using stats.fisher_exact from scipy v1.6.3. Calculation of cosine similarities: Mutations for
998 each strain were converted into a vector, with ordered values representing different mutation
999 categories as a proportion of total mutations. These were then compared in a pairwise fashion.

1000 Given two vectors A and B, the cosine similarity ($\cos(\theta)$) was calculated as:

$$\cos(\theta) = \frac{\sum_{i=1}^n A_i B_i}{\sqrt{\sum_{i=1}^n (A_i)^2} \sqrt{\sum_{i=1}^n (B_i)^2}}$$

1001

1002

1003 Hierarchical clustering used the hclust function of R (version 4.1.0) with complete linkage clustering
1004 of pairwise cosine distances (1 - cosine similarity) between ID-83 mutation spectra, with 41
1005 categories of productive reporter frameshift mutations. For bootstrap support, $n=1,000$ bootstrap
1006 datasets were generated by sampling with replacement the mutations observed with a strain, for
1007 each strain; then calculating the cosine distance and hierarchical clustering for each bootstrap

1008 dataset. Reported bootstrap scores are the percentage of bootstrap replicates hierarchical clustering
1009 of which supports the clustering to the right of the indicated position.

1010 To test significance of cosine similarities, we used a null model based on the Dirichlet-multinomial
1011 distribution. Briefly, when comparing two mutation count vectors, with total mutations m_1 and m_2 ,
1012 over n mutation classes, we constructed a distribution of cosine values by comparing 10,000
1013 simulated pairs of random vectors generated as follows. For each simulated pair, we sampled from a
1014 Dirichlet-multinomial distribution with the concentration parameters as a vector of ones of
1015 dimension n , and number of trials as m_1 for the first vector in the pair, and m_2 for the second vector.
1016 The null distribution was obtained by computing the cosine similarity of the 10,000 pairs of mutation
1017 count vectors.

1018

1019 **Additional References**

- 1020 51 Oceguera-Yanez, F. *et al.* Engineering the AAVS1 locus for consistent and scalable transgene
1021 expression in human iPSCs and their differentiated derivatives. *Methods* **101**, 43-55,
1022 doi:10.1016/j.ymeth.2015.12.012 (2016).
- 1023 52 Gritz, L. & Davies, J. Plasmid-encoded hygromycin B resistance: the sequence of hygromycin
1024 B phosphotransferase gene and its expression in *Escherichia coli* and *Saccharomyces*
1025 *cerevisiae*. *Gene* **25**, 179-188, doi:10.1016/0378-1119(83)90223-8 (1983).
- 1026 53 Brachmann, C. B. *et al.* Designer deletion strains derived from *Saccharomyces cerevisiae*
1027 S288C: A useful set of strains and plasmids for PCR-mediated gene disruption and other
1028 applications. *Yeast* **14**, 115-132, doi:10.1002/(SICI)1097-0061(19980130)14:2<115::AID-
1029 YEA204>3.0.CO;2-2 (1998).
- 1030 54 Spell, R. M. & Jinks-Robertson, S. 3-12 (Springer, 2004).
- 1031 55 Lea, D. E. & Coulson, C. A. The distribution of the numbers of mutants in bacterial
1032 populations. *Journal of Genetics* **49**, 264-285, doi:10.1007/BF02986080 (1949).
- 1033 56 Altman, D. G. *Practical statistics for medical research*. (Chapman and Hall, 1991).
- 1034 57 Vallot, C., Herault, A., Boyle, S., Bickmore, W. A. & Radvanyi, F. PRC2-independent chromatin
1035 compaction and transcriptional repression in cancer. *Oncogene* **34**, 741-751,
1036 doi:10.1038/onc.2013.604 (2015).
- 1037 58 Benitez-Guijarro, M. *et al.* RNase H2, mutated in Aicardi-Goutières syndrome, promotes
1038 LINE-1 retrotransposition. *The EMBO journal* **37**, doi:10.15252/embj.201798506 (2018).
- 1039 59 Reijns, M. A. M. *et al.* The Structure of the Human RNase H2 Complex Defines Key
1040 Interaction Interfaces Relevant to Enzyme Function and Human Disease. *Journal of Biological*
1041 *Chemistry* **286**, 10530-10539, doi:10.1074/jbc.M110.177394 (2011).

1042 60 Lujan, S. A. *et al.* Heterogeneous polymerase fidelity and mismatch repair bias genome
1043 variation and composition. *Genome research* **24**, 1751-1764, doi:10.1101/gr.178335.114
1044 (2014).

1045 61 Li, H. Aligning sequence reads, clone sequences and assembly contigs with BWA-MEM.
1046 (2013).

1047 62 Faust, G. G. & Hall, I. M. SAMBLASTER: fast duplicate marking and structural variant read
1048 extraction. *Bioinformatics* **30**, 2503-2505, doi:10.1093/bioinformatics/btu314 (2014).

1049 63 Van der Auwera, G. A. *et al.* From fastQ data to high-confidence variant calls: The genome
1050 analysis toolkit best practices pipeline. *Current Protocols in Bioinformatics* **43**,
1051 doi:10.1002/0471250953.bi1110s43 (2013).

1052 64 Van der Auwera, G. A. & O'Connor, B. D. *Genomics in the Cloud: Using Docker, GATK, and*
1053 *WDL in Terra*. (O'Reilly Media, 2020).

1054 65 Keane, T. M. *et al.* Mouse genomic variation and its effect on phenotypes and gene
1055 regulation. *Nature* **477**, 289-294, doi:10.1038/nature10413 (2011).

1056 66 Racz, C. *et al.* Isaac: ultra-fast whole-genome secondary analysis on Illumina sequencing
1057 platforms. *Bioinformatics* **29**, 2041-2043, doi:10.1093/bioinformatics/btt314 (2013).

1058 67 Roller, E., Ivakhno, S., Lee, S., Royce, T. & Tanner, S. Canvas: versatile and scalable detection
1059 of copy number variants. *Bioinformatics* **32**, 2375-2377, doi:10.1093/bioinformatics/btw163
1060 (2016).

1061 68 Robinson, J. T. *et al.* Integrative genomics viewer. *Nat Biotechnol* **29**, 24-26,
1062 doi:10.1038/nbt.1754 (2011).

1063 69 Nik-Zainal, S. *et al.* The life history of 21 breast cancers. *Cell* **149**, 994-1007,
1064 doi:10.1016/j.cell.2012.04.023 (2012).

1065 70 Raine, K. M. *et al.* ascatNgs: Identifying Somatic Copy-Number Alterations from
1066 Whole-Genome Sequencing Data. *Curr Protoc Bioinformatics* **56**, 15 19 11-15 19 17,
1067 doi:10.1002/cpbi.17 (2016).

1068 71 Sekhon, J. S. Multivariate and Propensity Score Matching Software with Automated Balance
1069 Optimization: The Matching package for R. *Journal of Statistical Software* **42**, 1 - 52,
1070 doi:10.18637/jss.v042.i07 (2011).

1071 72 Benjamin, D. *et al.* Calling Somatic SNVs and Indels with Mutect2. *bioRxiv*, 861054,
1072 doi:10.1101/861054 (2019).

1073 73 McKenna, A. *et al.* The Genome Analysis Toolkit: a MapReduce framework for analyzing
1074 next-generation DNA sequencing data. *Genome Res* **20**, 1297-1303,
1075 doi:10.1101/gr.107524.110 (2010).

1076 74 Kim, S. *et al.* Strelka2: fast and accurate calling of germline and somatic variants. *Nat*
1077 *Methods* **15**, 591-594, doi:10.1038/s41592-018-0051-x (2018).

1078 75 Wala, J. A. *et al.* SvABA: genome-wide detection of structural variants and indels by local
1079 assembly. *Genome Res* **28**, 581-591, doi:10.1101/gr.221028.117 (2018).

1080 76 Rimmer, A. *et al.* Integrating mapping-, assembly- and haplotype-based approaches for
1081 calling variants in clinical sequencing applications. *Nat Genet* **46**, 912-918,
1082 doi:10.1038/ng.3036 (2014).

1083 77 Danecek, P. *et al.* Twelve years of SAMtools and BCFtools. *Gigascience* **10**,
1084 doi:10.1093/gigascience/giab008 (2021).

1085 78 Karczewski, K. J. *et al.* The mutational constraint spectrum quantified from variation in
1086 141,456 humans. *Nature* **581**, 434-443, doi:10.1038/s41586-020-2308-7 (2020).

1087 79 Chen, X. *et al.* Manta: rapid detection of structural variants and indels for germline and
1088 cancer sequencing applications. *Bioinformatics* **32**, 1220-1222,
1089 doi:10.1093/bioinformatics/btv710 (2016).

1090 80 Xia, B. *et al.* Widespread Transcriptional Scanning in the Testis Modulates Gene Evolution
1091 Rates. *Cell* **180**, 248-262 e221, doi:10.1016/j.cell.2019.12.015 (2020).

1092 81 Consortium, F. *et al.* A promoter-level mammalian expression atlas. *Nature* **507**, 462-470,
1093 doi:10.1038/nature13182 (2014).

1094 82 Karimzadeh, M., Ernst, C., Kundaje, A. & Hoffman, M. M. Umap and Bimap: quantifying
1095 genome and methylome mappability. *Nucleic Acids Res* **46**, e120, doi:10.1093/nar/gky677
1096 (2018).

1097 83 Bergstrom, E. N. *et al.* SigProfilerMatrixGenerator: A tool for visualizing and exploring
1098 patterns of small mutational events. *BMC Genomics* **20**, 685-685, doi:10.1186/s12864-019-
1099 6041-2 (2019).

1100 84 Tareen, A. & Kinney, J. B. Logomaker: beautiful sequence logos in Python. *Bioinformatics* **36**,
1101 2272-2274, doi:10.1093/bioinformatics/btz921 (2020).

1102 85 Reijns, M. A. M. *et al.* Lagging-strand replication shapes the mutational landscape of the
1103 genome. *Nature* **518**, 502-506, doi:10.1038/nature14183 (2015).

1104 86 Ding, J., Taylor, M. S., Jackson, A. P. & Reijns, M. A. M. Genome-wide mapping of embedded
1105 ribonucleotides and other noncanonical nucleotides using emRiboSeq and EndoSeq. *Nature*
1106 *protocols* **10**, 1433-1444, doi:10.1038/nprot.2015.099 (2015).

1107 87 Quinlan, A. R. & Hall, I. M. BEDTools: a flexible suite of utilities for comparing genomic
1108 features. *Bioinformatics* **26**, 841-842, doi:10.1093/bioinformatics/btq033 (2010).

1109 88 Kornberg, A., Bertsch, L. L., Jackson, J. F. & Khorana, H. G. Enzymatic Synthesis of
1110 Deoxyribonucleic Acid, Xvi. Oligonucleotides as Templates and the Mechanism of Their
1111 Replication. *Proc Natl Acad Sci U S A* **51**, 315-323, doi:10.1073/pnas.51.2.315 (1964).

1112 89 Fan, H. & Chu, J. Y. A brief review of short tandem repeat mutation. *Genomics Proteomics*
1113 *Bioinformatics* **5**, 7-14, doi:10.1016/S1672-0229(07)60009-6 (2007).

1114 90 Stok, C., Kok, Y. P., van den Tempel, N. & van Vugt, M. Shaping the BRCAness mutational
1115 landscape by alternative double-strand break repair, replication stress and mitotic
1116 aberrancies. *Nucleic Acids Res* **49**, 4239-4257, doi:10.1093/nar/gkab151 (2021).

1117 91 Drost, J. *et al.* Use of CRISPR-modified human stem cell organoids to study the origin of
1118 mutational signatures in cancer. *Science* **358**, 234-238, doi:10.1126/science.aao3130 (2017).

1119 92 Hiller, B. *et al.* Mammalian RNase H2 removes ribonucleotides from DNA to maintain
1120 genome integrity. *The Journal of Experimental Medicine* **209**, 1419-1426,
1121 doi:10.1084/jem.20120876 (2012).

1122

1123 Acknowledgments

1124 We are grateful to Sue Jinks-Robertson for suggesting the traffic light reporter approach, Hannah
1125 Klein for guidance on fluctuation assays, Ruben van Boxtel for sharing sequencing data for MLH1-KO
1126 organoids, Andy Bretherick, Oscar Bedoya Reina and Greg Kudla for advice on HygroR re-coding. We
1127 thank IGC core services (Laura Murphy, Craig Nicol, Connor Warnock, Elisabeth Freyer, Stephen
1128 Brown, Jeffrey Joseph), Clare Logan, Adeline Fluteau, Andrea Robertson and Edinburgh Genomics,
1129 for technical assistance; Liverpool CLL biobank (funded by Blood Cancer UK) for samples used to
1130 generate GEL WGS data; Ailith Ewing, Carol-Anne Martin and Wendy Bickmore for discussions.
1131 Funding for this work: UK Medical Research Council Human Genetics Unit core grants

1132 (MC_UU_00007/5 to APJ, MC_UU_00007/11 to MST); Edinburgh Clinical Academic Track PhD
1133 programme (Wellcome Trust 204802/Z/16/Z) to TCW; 2021 AACR-Amgen Fellowship in
1134 Clinical/Translational Cancer Research (Grant Number 21-40-11-NADE) to FN; a CRUK Brain Tumour
1135 Centre of Excellence Award (C157/A27589) to MDN; EKFS research grant (2019_A09), Wilhelm
1136 Sander-Stiftung (2019.046.1) to KA, CRUK programme grant (C20807/A2864) to TS; "la Caixa"
1137 Foundation (CLLEvolution-LCF/PR/HR17/52150017, Health Research 2017 Program HR17-00221) to
1138 EC. EC is an Academia Researcher of the "Institució Catalana de Recerca i Estudis Avançats" of the
1139 Generalitat de Catalunya. Edinburgh Genomics is partly supported by NERC (R8/H10/56), MRC
1140 (MR/K001744/1) and BBSRC (BB/J004243/1). This research was made possible through access to the
1141 data and findings generated by the 100,000 Genomes Project. The 100,000 Genomes Project is
1142 managed by Genomics England Limited (a wholly owned company of the Department of Health and
1143 Social Care). The 100,000 Genomes Project is funded by the National Institute for Health Research
1144 and NHS England. The Wellcome Trust, Cancer Research UK and the Medical Research Council have
1145 also funded research infrastructure. The 100,000 Genomes Project uses data provided by patients
1146 and collected by the National Health Service as part of their care and support.

1147

1148 **Author Contributions**

1149 M.A.M.R, T.C.W., M.S.T. and A.P.J. conceived the project and designed the experiments. T.C.W. and
1150 M.A.M.R, with help from P.C., performed fluctuation assays and sequencing experiments. M.A.M.R.,
1151 with help from P.C., performed the RPE1 mutation accumulation experiment. S.B. performed FISH
1152 experiments. M.A.M.R., T.C.W. and D.O.R.S. performed all other molecular biology experiments. H.X.
1153 and K.A. provided mouse tumour and control tissue samples. D.A.P., T.C.W., M.D.N. and M.S.T.
1154 designed and implemented computational analyses. D.A.P., T.C.W. and M.S.T analysed yeast, mouse,
1155 RPE1 and Gene4Denovo WGS data. D.A.P. and M.S.T. performed pan-cancer analyses. T.G.E.R.C., K.R
1156 and A.S. provided CLL WGS data. A.J.C. provided CRC data. D.A.P., F.N., R.L.H., R.R. and C.P. analysed

1157 CLL data. D.A.P. analysed CRC data. M.A.M.R, C.P., T.S., E.C, M.S.T. and A.P.J. supervised the work.
1158 T.C.W., F.N., E.C., T.S., M.S.T. and A.P.J. funded the work. M.A.M.R. and A.P.J. wrote the manuscript.
1159 All authors had the opportunity to edit the manuscript. All authors approved the final manuscript.

1160

1161 **Competing interests**

1162 The authors declare no competing interests.

1163

1164 **Additional information**

1165 Supplementary Information is available for this paper.

1166 Correspondence and requests for materials should be addressed to Martin A.M. Reijns, Martin S.
1167 Taylor or Andrew P. Jackson

1168 Peer review information

1169 Reprints and permissions information is available at www.nature.com/reprints

1170

1171 **Data Availability**

1172 RPE1 mutation accumulation experiment and mouse tumour WGS data are available from European
1173 Nucleotide Archive accession PRJEB48753 (<https://www.ebi.ac.uk/ena/browser/view/PRJEB48753>).

1174 All other data were previously published and sources are cited in Supplementary Table 5.

1175

1176 **Code Availability**

1177 Code documented in Methods is available at <https://git.ecdf.ed.ac.uk/ID-TOP1>

1178

1179 **The Genomics England Research Consortium**

1180 John C. Ambrose¹⁵, Prabhu Arumugam¹⁵, Roel Bevers¹⁵, Marta Bleda¹⁵, Freya Boardman-Pretty^{15,16},
1181 Christopher R. Boustred¹⁵, Helen Brittain¹⁵, Mark J. Caulfield^{15,16}, Georgia C. Chan¹⁵, Greg Elgar^{15,16},
1182 Tom Fowler¹⁵, Adam Giess¹⁵, Angela Hamblin¹⁵, Shirley Henderson^{15,16}, Tim J.P. Hubbard¹⁵, Rob
1183 Jackson¹⁵, Louise J. Jones^{15,16}, Dalia Kasperaviciute^{15,16}, Melis Kayikci¹⁵, Athanasios Kousathanas¹⁵, Lea
1184 Lahnstein¹⁵, Sarah E.A. Leigh¹⁵, Ivonne U.S. Leong¹⁵, Javier F. Lopez¹⁵, Fiona Maleady-Crowe¹⁵, Meriel
1185 McEntagart¹⁵, Federico Minneci¹⁵, Loukas Moutsianas^{15,16}, Michael Mueller^{15,16}, Nirupa Murugaesu¹⁵,
1186 Anna C. Need^{15,16}, Peter O'Donovan¹⁵, Chris A. Odhams¹⁵, Christine Patch^{15,16}, Mariana Buongermino
1187 Pereira¹⁵, Daniel Perez-Gil¹⁵, John Pullinger¹⁵, Tahrima Rahim¹⁵, Augusto Rendon¹⁵, Tim Rogers¹⁵,
1188 Kevin Savage¹⁵, Kushmita Sawant¹⁵, Richard H. Scott¹⁵, Afshan Siddiq¹⁵, Alexander Sieghart¹⁵, Samuel
1189 C. Smith¹⁵, Alona Sosinsky^{15,16}, Alexander Stuckey¹⁵, Mélanie Tanguy¹⁵, Ana Lisa Taylor Tavares¹⁵,
1190 Ellen R. A. Thomas^{15,16}, Simon R. Thompson¹⁵, Arianna Tucci^{15,16}, Matthew J. Welland¹⁵, Eleanor
1191 Williams¹⁵, Katarzyna Witkowska^{15,16}, Suzanne M. Wood^{15,16}.

1192

1193 ¹⁵ Genomics England, London, UK

1194 ¹⁶ William Harvey Research Institute, Queen Mary University of London, London, UK

1195

1196 **Colorectal Cancer Domain UK 100,000 Genomes Project**

1197 Daniel Chubb⁹, Alex Cornish⁹, Ben Kinnersley⁹, Richard Houlston⁹, David Wedge¹⁷, Andreas Gruber¹⁷,
1198 Anna Frangou¹⁸, William Cross¹⁹, Trevor Graham²⁰, Andrea Sottoriva⁹, Gulio Caravagna⁹, Nuria Lopez-
1199 Bigas²¹, Claudia Arnedo Pac²¹, David Church¹⁸, Richard Culliford⁹, Steve Thorn²², Phil Quirke²³, Henry
1200 Wood²³, Ian Tomlinson²², Boris Noyvert⁵

1201

1202 ¹⁷ Manchester Interdisciplinary Biocentre, University of Manchester, Manchester, UK
1203 ¹⁸ Wellcome Centre for Human Genetics, Oxford, UK
1204 ¹⁹ Cancer Institute, University College London, London, UK
1205 ²⁰ Barts Cancer Institute, Barts and The London School of Medicine and Dentistry, Queen Mary
1206 University of London, London, UK
1207 ²¹ Institute for Research in Biomedicine (IRB Barcelona), The Barcelona Institute of Science and
1208 Technology (BIST), Barcelona, Spain
1209 ²² Edinburgh Cancer Research Centre, IGC, The University of Edinburgh, Edinburgh, UK
1210 ²³ Pathology and Data Analytics, Leeds Institute of Medical Research, St James's University Hospital,
1211 University of Leeds, Leeds, UK

1212

1213 **Extended data figure legends**

1214 **Extended Data Fig. 1 | ID4 is distinct from small deletion signatures of known aetiology. a,b,** The
1215 mechanistic basis for many COSMIC indel signatures is unknown, with only 9 out of 18 having a
1216 proposed aetiology. ID2 (**a**) is attributed to DNA polymerase slippage^{88,89} and ID6 (**b**) to
1217 microhomology mediated end-joining (MMEJ) activity, associated with HR deficiency^{5,90}. **c,d,**
1218 Mechanism for these signatures supported by: impaired MMR promoting replication slippage
1219 mutagenesis in MLH1^{-/-} colonic organoids resulting in ID2 (and ID1) signatures (**c**); ID6 contributing
1220 substantially (along with ID8) to the indel signature in ovarian cancer, in which HR deficiency is
1221 common (**d**). Analysis of data from⁹¹ in **c**; data for 73 ovarian adenocarcinomas with ID6
1222 contribution from ICGC^{5,50} in **d**.

1223

1224 **Extended Data Fig. 2 | Yeast and human frameshift mutation reporters detect indels at tandem**
1225 **repeats. a,** Yeast reporter. Synonymous substitutions were made in the hygromycin resistance gene

1226 (HygroR), such that it contained many short 2 bp tandem repeats (SSTRs). Expression from the TEF
1227 promoter (P_{TEF}) ensures a constitutive high level of transcription. Mutations within HygroR that
1228 result in a frameshift simultaneously put the HygroR coding sequence out of frame and the
1229 downstream neomycin resistance (NeoR) sequence in frame, allowing antibiotic selection of cells
1230 with such mutations. **b**, Top1-dependent 2 bp SSTR deletions occur in both WT and *rnh201Δ* (RNase
1231 H2 null) yeast, with the highest mutation rate for *rnh201Δ* (related to Fig. 1d). **c-e**, WT and *rnh201Δ*
1232 have similar spectra, and differ from *top1Δ* strains. Mutation spectra of neomycin resistant colonies.
1233 n, number of independent colonies sequenced. Other: complex indels, missense mutations or
1234 mutation not characterised (**c**). Tree for pairwise clustering with percent bootstrap support to the
1235 right of the indicated position, based on cosine scores calculated for mutation spectra (Fig. 1e) of the
1236 41 mutation categories that give productive reporter frameshift mutations (**d**). Matrix of pairwise
1237 cosine similarities and P-values between reporter mutation spectra in different yeast strains. Darker
1238 blue indicates greater similarity; darker grey greater significance. Test statistic is the cosine similarity
1239 value for 41 mutation categories and the null hypothesis is that that the cosine value will be
1240 distributed according to the Dirichlet-multinomial model, as described in Methods. The test is one-
1241 sided and no adjustments were made for multiple comparisons (**e**). **f**, Null distribution for cosine
1242 pairwise vector comparisons for 41 and 83 mutation categories. Plots, cosine values for 10,000
1243 randomly generated pairs of vectors of mutation spectra. Each vector contained 100 randomly
1244 assigned mutations (see Methods for further details). Cosine value thresholds indicated for $P < 0.05$
1245 and $P < 0.01$. **g**, The human reporter is expressed from the ubiquitous CAG promoter (P_{CAG}), and
1246 NeoR is replaced with the puromycin resistance gene (PuroR) to allow more rapid antibiotic
1247 selection in mammalian cell culture.

1248

1249 **Extended Data Fig. 3 | Validation and characterisation of RNASEH2A+ and KO HeLa reporter cells.**

1250 **a-c**, Reporter integration at the *AAVS1* locus and retention of a reporter-free locus with a 200 bp

1251 deletion at the target site was confirmed by PCR and Sanger sequencing. Green arrow head, specific
1252 PCR product. Representative of at least 2 independent experiments. **d,e**, FISH shows integration of
1253 the reporter (**d**) at a single *AAVS1* locus (**e**). Representative image of approximately one hundred
1254 mitotic chromosome spreads in 3 independent experiments. SA, splice acceptor; T2A, self-cleaving
1255 peptide; pA, polyadenylation site; also see [Fig. 2a](#). **f,g**, Alkaline gel electrophoresis of RNase H2
1256 treated genomic DNA (**f**) shows a small increase in fragmentation for the RNASEH2A+ control clone
1257 and a more substantial increase in two independent RNASEH2A-KO clones (representative of 4
1258 independent experiments), indicating the presence of more genome-embedded ribonucleotides
1259 compared to HeLa and parental reporter cells (**g**). “Control KO” cells were reported previously^{33,58}.
1260 RFU, relative fluorescence units. **h**, 2 bp SSTR deletions are frequent in both RNASEH2A+ and KO
1261 cells. Mutation spectra, quantitation of indel type. Relative area of pie charts scaled to mutation
1262 rate. n, number of colonies sequenced from independent cultures. Other: complex indels or
1263 missense mutations.

1264

1265 **Extended Data Fig. 4 | RPE1 RNase H2 null cells accumulate embedded ribonucleotides and 2-5 bp**
1266 **deletions across the genome. a,b**, *RNASEH2A* and *RNASEH2B* KO cells (AKO, BKO, respectively) have
1267 substantially reduced cellular levels of RNase H2 subunits (**a**) and are deficient for RNase H2 enzyme
1268 activity (**b**) at the outset (ancestral) and at the end of the mutation accumulation experiment (end
1269 point). Individual data points, $n=3$ technical replicates; mean \pm s.d. For gel source data, see
1270 [Supplementary Fig. 1](#). **c,d**, Alkaline gel electrophoresis of RNase H2 treated genomic DNA (**c**) shows a
1271 substantial increase in fragmentation for *RNASEH2A* and *RNASEH2B* KO clones (representative of 3
1272 independent experiments), indicating the presence of more genome-embedded ribonucleotides
1273 compared to two WT control clones (**d**). Densitometry plots of **c**. RFU, relative fluorescence units. As
1274 RNase H2 deficiency activates the p53 pathway^{14,92}, experiments were performed in a *TP53* knockout
1275 background. **e**, Only 2-5 bp deletions are significantly increased in RNase H2 null cells. Data points

1276 for acquired indel mutations in individual cell lines after 100 population doublings. Individual data
1277 points, indel counts per cell line; mean \pm s.d.; P-values for two-sided Fisher's exact test between WT
1278 ($n=3$ independent clones) and KO ($n=2$ independent clones) for one indel type vs all other indel
1279 types, after Bonferroni correction. **f**, Proportions of acquired indels in WT and KO RPE cells. After
1280 correction for indels occurring in WT, 69% of indels in RNase H2 null cells are 2-5 bp deletions. n ,
1281 total indel counts. **g**, Quantification of 2 bp deletions by context. n , total number of 2 bp deletions.
1282 For **f** and **g**, chart areas scaled to mutation counts per line.

1283

1284 **Extended Data Fig. 5 | ID4 occurs in RNase H2 null RPE1 cells, particularly in transcribed regions. a-**

1285 **d**, Mutational spectra detected by WGS after 100 population doublings in RPE1 cells demonstrates
1286 that SSTR and SNMH/MH deletions are enriched in RNase H2 cells. Spectra for combined RNase H2
1287 null and wildtype cell lines (**a**), and individual cell lines (**b**). Mutational signature analysis confirms
1288 ID4 contribution in RNase H2 null (**c**), but not WT cells (**d**). **e**, In RNase H2 null cells, ID4 contributes
1289 significantly more to indel mutations in transcribed genomic regions ($P=1.3 \times 10^{-29}$). Two-sided
1290 Fisher's exact test, ID4 indels vs other indels.

1291

1292 **Extended Data Fig. 6 | ID4 mutations in RNase H2 null mouse tumours and RPE1 cells occur at a**

1293 **TNT motif, defining ID-TOP1. a**, Mutation spectra for individual Rnaseh2b-KO murine intestinal
1294 tumours (WGS, paired tumour-normal samples from 6 mice). **b**, Indel classes, detected in murine
1295 Rnaseh2b-KO tumours. n , total indel count for 6 tumours. **c**, Most 2 bp deletions in these tumours
1296 occur at SSTRs and sites of single nucleotide microhomology (SNMH). n , number of 2 bp deletions.
1297 **d,e**, A TNT sequence motif is present at all 2 bp STR and SNMH deletions in RNase H2 null mouse
1298 tumours (**d**) and RPE1 cells (**e**). Related to [Fig. 4d](#) and [Fig. 3](#), respectively. Sequence logo: 2-bit
1299 representation of the sequence context of 2 bp deletions. Top, all deletions, with those sequences
1300 containing a deleted adenosine (except AT/TA) reverse complemented, and deletions right-aligned.

1301 Middle, re-aligned on right-hand T. Bottom, aligned on T (STR and SNMH context only). n, number of
1302 deletions. **f**, Deletion sites in RNase H2 null RPE1 cells are significantly enriched for the TNT
1303 sequence motif compared to genome-wide occurrence, for all genome sequence, as well as SNMH
1304 sites. P-values, two-sided Fisher's exact, observed vs expected. $n=98$ (all; $P=8.3 \times 10^{-14}$), 54 (STR;
1305 $P=0.057$), 30 (SNMH; $P=0.0008$) deletions.

1306

1307 **Extended Data Fig. 7 | ID4 deletions in RNase H2 null *S. cerevisiae* occur at a TNT motif in a Top1-**
1308 **dependent manner. a**, 2 bp deletion sites in *rnh201Δ pol2-M644G* yeast are significantly enriched
1309 for the TNT sequence motif compared to genome-wide occurrence, for all genome sequence, as well
1310 as STR sites. P-values, two-sided Fisher's exact, observed vs expected. $n=94$ (all; $P=1.0 \times 10^{-9}$), 91 (STR;
1311 $P=0.029$), 3 (SNMH; $P=1$) deletions. **b**, A TNT sequence motif is present at all 2 bp STR and SNMH
1312 deletions in *rnh201Δ pol2-M644G* yeast. Sequence logo: 2-bit representation of the sequence
1313 context of 2 bp deletions. Top, all deletions, with those sequences containing a deleted adenosine
1314 (except AT/TA) reverse complemented, and deletions aligned on right-hand T. Bottom, aligned on T
1315 (STR and SNMH context only). n, number of deletions. **c,d**, TN*T motifs extend beyond 2 bp
1316 deletions, with enrichment above expectation for 2 bp deletions at TNT, 3 bp deletions at TNNT and
1317 4 bp deletions at TNNNT motifs in *rnh201Δ pol2-M644G* yeast WGS. Null expectations were
1318 generated by randomly simulating deletions of 2, 3 and 4 bp (**c**) or 2 bp STR sequences (**d**) genome-
1319 wide and scoring those simulated events for TN*T compliance. Each simulated dataset matched the
1320 count of observed mutations for the corresponding deletion class and $n=1,000$ replicate simulated
1321 datasets were produced. The frequency distribution of TN*T compliance in simulations is plotted as
1322 histograms, and comparison to the observed frequency of TN*T compliance (dotted red lines) used
1323 to derive a two-tailed empirical P-value. **e**, 2 bp STR deletions have biased sequence composition.
1324 Deletion observed in *rnh201Δ pol2-M644G* yeast WGS. Genome, frequency of dinucleotides in STR
1325 sequences in mappable genome. **f**, Ribouridine (rU) is more common in a CrU/GrU than in an

1326 ArU/TrU dinucleotide context. Genome-embedded ribonucleotide frequency determined by
1327 emRiboSeq⁸⁶. Dotted line indicates relative rate in absence of bias (=0.25). Horizontal lines, mean;
1328 individual data points, values for $n=4$ independent experiments⁸⁵. **g,h**, 2 bp TNT deletions in wildtype
1329 and RNase H2 null cells are dependent on Topoisomerase 1. Mutation rates for 2 bp deletions at
1330 TNT-compliant SSTRs (**g**). Deletions at TNT motifs are significantly increased above expectation in WT
1331 and *rnh201Δ*, but not in *top1Δ* and *rnh201Δ top1Δ* yeast. Horizontal bars, 95% confidence intervals
1332 for odds ratio estimates (diamonds). P-values, two-sided Fisher's exact after Bonferroni correction;
1333 $n=86, 28, 103, 19$ 2-bp deletions, with each deletion from an independent culture, for WT, *top1Δ*,
1334 *rnh201Δ*, *rnh201Δ top1Δ*, respectively. Null expectation, random occurrence of mutations in
1335 reporter target sequence (**h**).

1336

1337 **Extended Data Fig. 8 | TOP1-mediated mutagenesis causes increased 2-5 bp deletions in cancer. a,**

1338 Of all indels, only 2-5 bp deletions are significantly increased in CLL with biallelic *RNASEH2B* loss.

1339 Box, 25-75%; line, median; whiskers 5-95% with data points for values outside this range. WT (2

1340 copies), $n=201$; monallelic loss (1 copy), $n=131$; biallelic loss (0 copies), $n=16$ independent tumours.

1341 Indels as percentage of all variants per sample (GEL and ICGC data combined). q-values, 2-sided

1342 Mann-Whitney test with 5% FDR. **b,c**, In RNase H2 null CLL, 2 bp deletions predominantly occur at

1343 STR and SNMH sequences (**b**), and at the TNT sequence motif (**c**), consistent with TOP-mediated

1344 mutagenesis. Mean \pm s.e.m., percentage of all variants per sample. GEL and ICGC data combined. $n=$

1345 1,711; 1,244; 443 2-bp indels identified in 201, 131, 16 biologically independent tumours,

1346 respectively. **d**, ID4 contribution in RNase H2 null CLL is greater in transcribed regions. Two-sided

1347 Fisher's exact test, ID4 indels vs other indels ($P=9.2 \times 10^{-16}$). **e**, Pan-cancer transcript expression data

1348 divided into ten expression strata for ubiquitously expressed genes (used in panel **h** and [Fig. 5b](#)

1349 analysis). Data points, median/maximum expression across cancer types for individual genes. Genes

1350 with similar median and maximum TPMs were considered to be ubiquitously expressed and divided

1351 into expression groups from low (1) to high (10) expression. **f**, Two bp deletions in cancer
1352 preferentially occur at STRs. **g**, ID-TOP1 deletions increase in frequency with TOP1 cleavage activity
1353 (measured by TOP1-Seq; ³⁸). Dotted line, relative rate in lowest TOP1-seq category set to 1. Solid
1354 lines, relative deletion rate. ID-TOP1, 2-5 bp MH and SSTR deletions containing the TN*T sequence
1355 motif. **h**, ID-TOP1, but not deletions in other sequence contexts, correlate with transcription. **i**, 2-5
1356 bp deletions from prostate adenocarcinoma are most enriched amongst the top 10% of highly
1357 expressed prostate 'tissue-restricted' genes. Odds ratio (OR): number of 2-5bp deletions in top 10%
1358 tissue restricted genes vs deletions in other genes, relative to expected frequency from all other
1359 tissues. **j**, ID4 is not detected in the indel signature of irinotecan-treated colorectal cancers.
1360 Untreated ($n=78$), treated ($n=39$). **k**, 2-5 bp deletion frequency in cancer corresponds to TOP1
1361 cleavage activity, in both genic and non-genic regions. Data analysed from PCAWG⁵⁰, all tumours in
1362 **e, h**; ID4 positive tumours in **g, k**; Genomics England in **j**. In **g, h** and **k**, solid line, relative deletion
1363 rate; shading indicates 95% confidence intervals from 1,000 (**g,k**) or 100 (**h**) bootstrap replicates.

1364

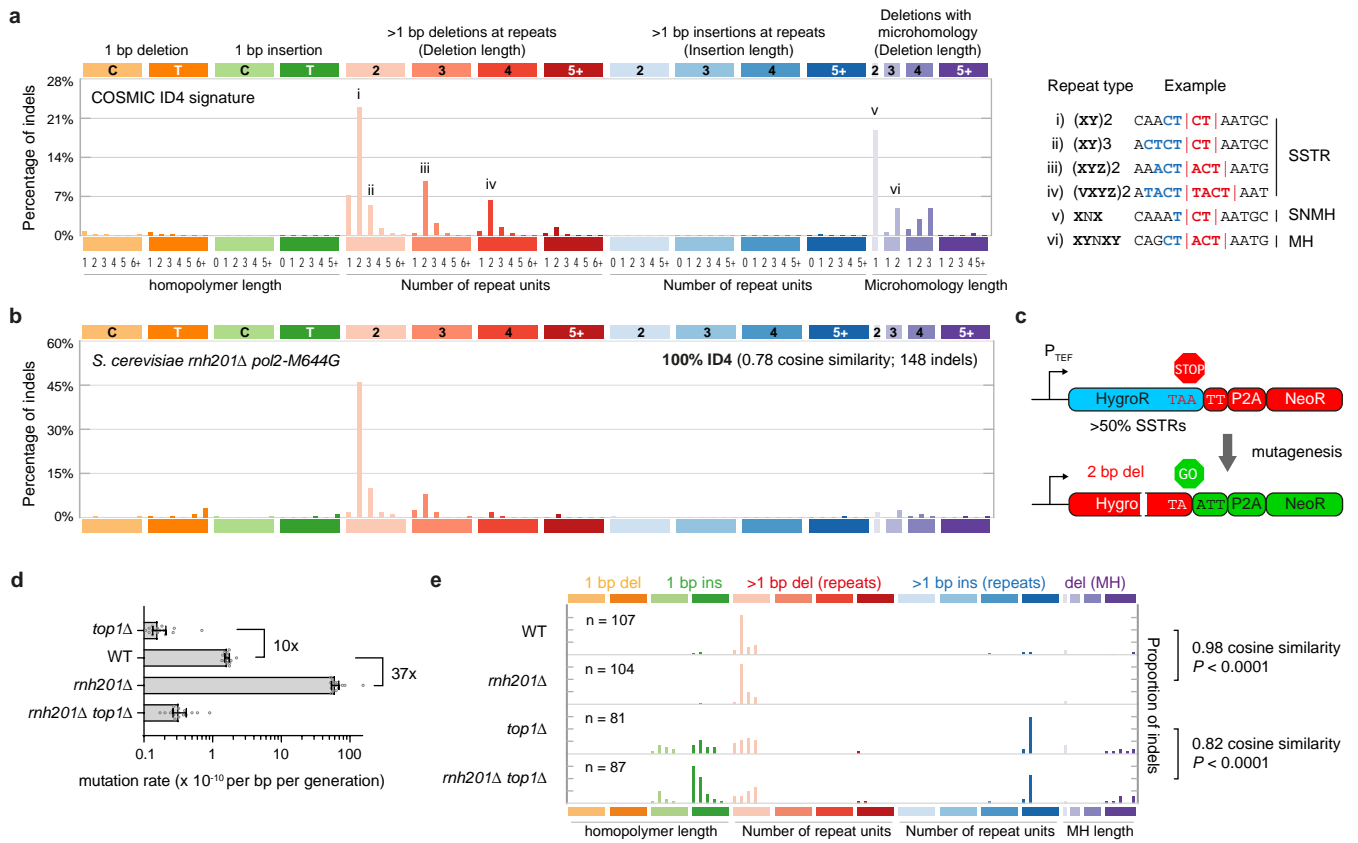
1365 **Extended Data Fig. 9 | Human germline *de novo* indels are enriched for ID-TOP1 deletions.** **a**, Most
1366 *de novo* 2 bp deletions occur at SSTR, STR and SNMH sequences. **b,c**, A TNT sequence motif is
1367 present at the majority of 2 bp STR and SNMH deletions (**b**). Sequence logos: 2-bit representation of
1368 the sequence context of 2 bp deletions. Top, all deletions, with those containing A (except AT/TA)
1369 reverse complemented, and deletions right-aligned on T (where present). Bottom, STR/SNMH
1370 deletions only (**c**). **d**, TN*T motifs extend beyond 2 bp deletions, with enrichment above expectation
1371 for 2 bp deletions at TNT, 3 bp deletions at TNNT and 4 bp deletions at TNNNT motifs ($P < 0.001$;
1372 two-tailed empirical P-value determined for each category). Bootstrap sampling ($n=1,000$) of 2, 3
1373 and 4 bp STR/MH sequences genome-wide to derive expected frequencies of those matching TN*T
1374 motifs. Sampling was performed to match the numbers of deletions at repeats observed in the
1375 Gene4Denovo database for each category defined by repeat type, repeat unit length and total

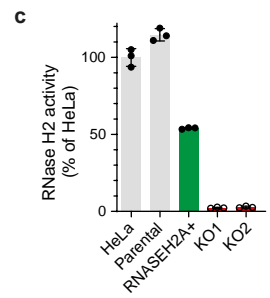
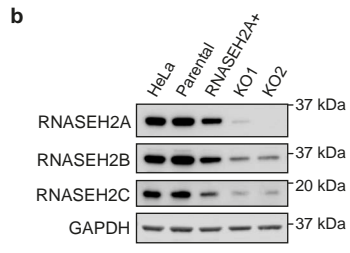
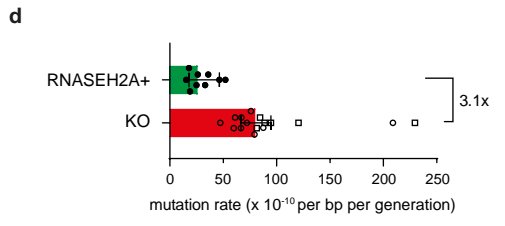
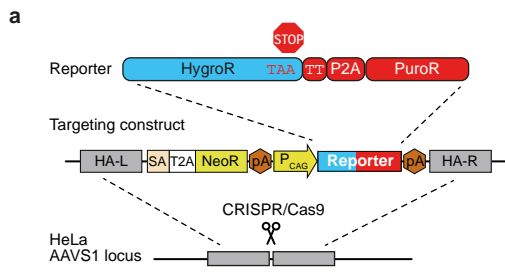
1376 repeat length. Histograms, distribution of the number of repeats matching TN*T motifs over these
1377 samplings. Solid blue lines, kernel density estimates for these distributions. Dotted red lines, number
1378 of deletions observed in Gene4Denovo matching TN*T motifs for each category. **e**, ID-TOP1
1379 correlates with germline expression level. ID-TOP1, defined as 2-5 bp MH and SSTR deletions
1380 containing the TN*T sequence motif. Shading, 95% confidence intervals from 100 bootstrap
1381 replicates.

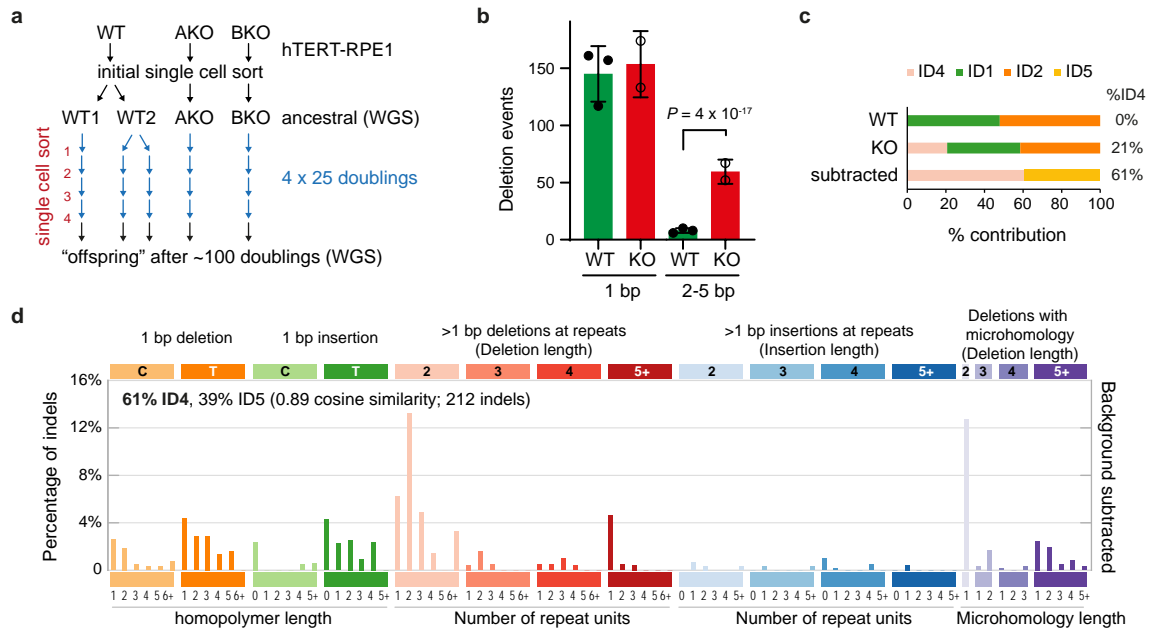
1382

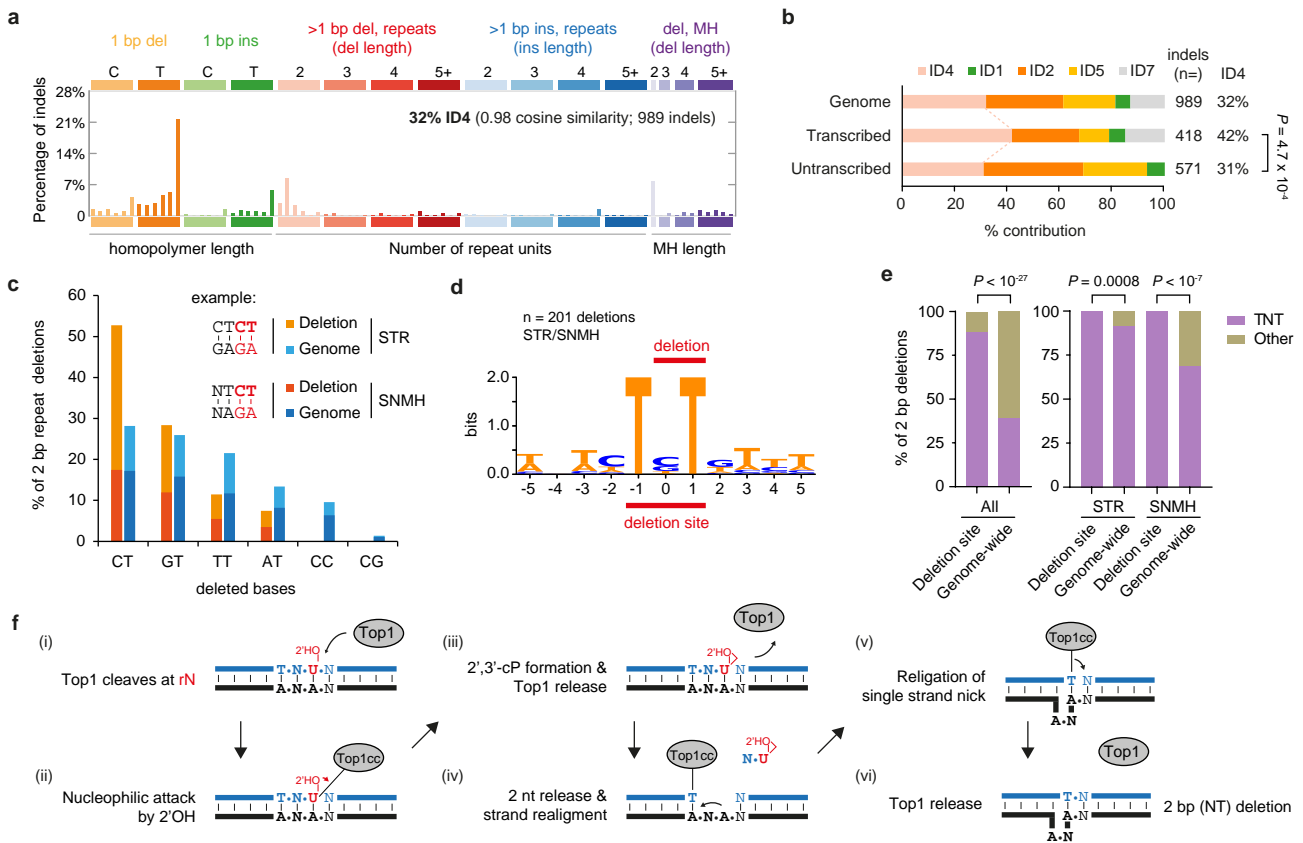
1383 **Extended Data Fig. 10 | Topoisomerase 1 causes small deletions while protecting against**

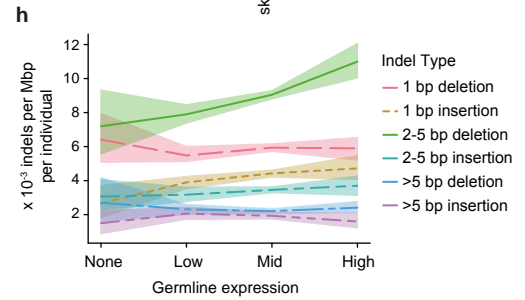
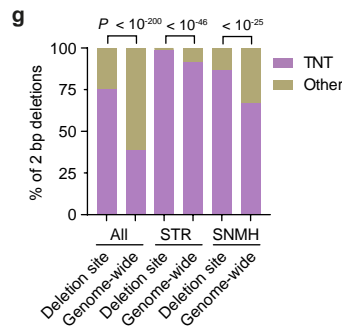
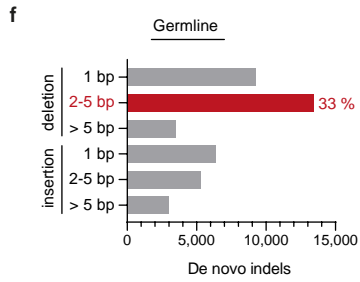
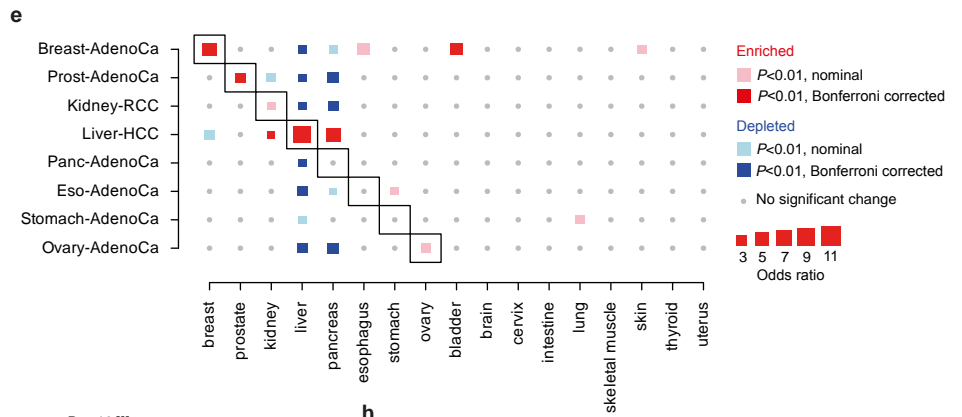
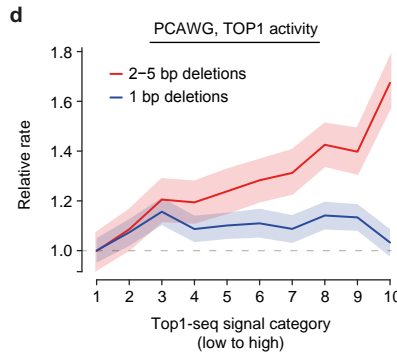
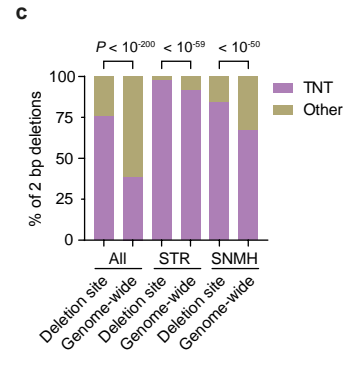
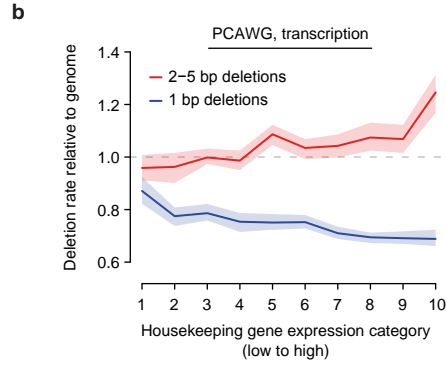
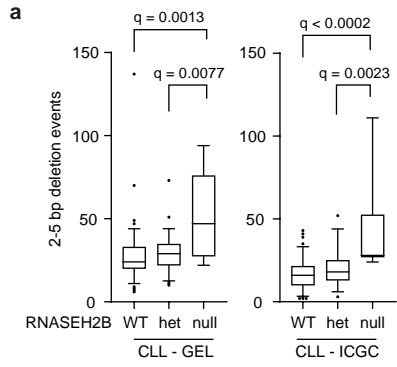
1384 **topological stress. a**, The canonical role of Topoisomerase 1 (TOP1) is to relieve torsional stress (sc,
1385 supercoiling) during replication and transcription. **b**, TOP1 acts by forming ssDNA nicks to release
1386 supercoils and then religates the relaxed DNA. However, TOP1 cleavage at genome-embedded
1387 ribonucleotides (frequently incorporated by replicative polymerases such as Pol ϵ), can lead to short
1388 deletions that will be most frequent at sites of torsional stress in the genome, such as occurs at
1389 highly transcribed genes. Adapted from ⁶.

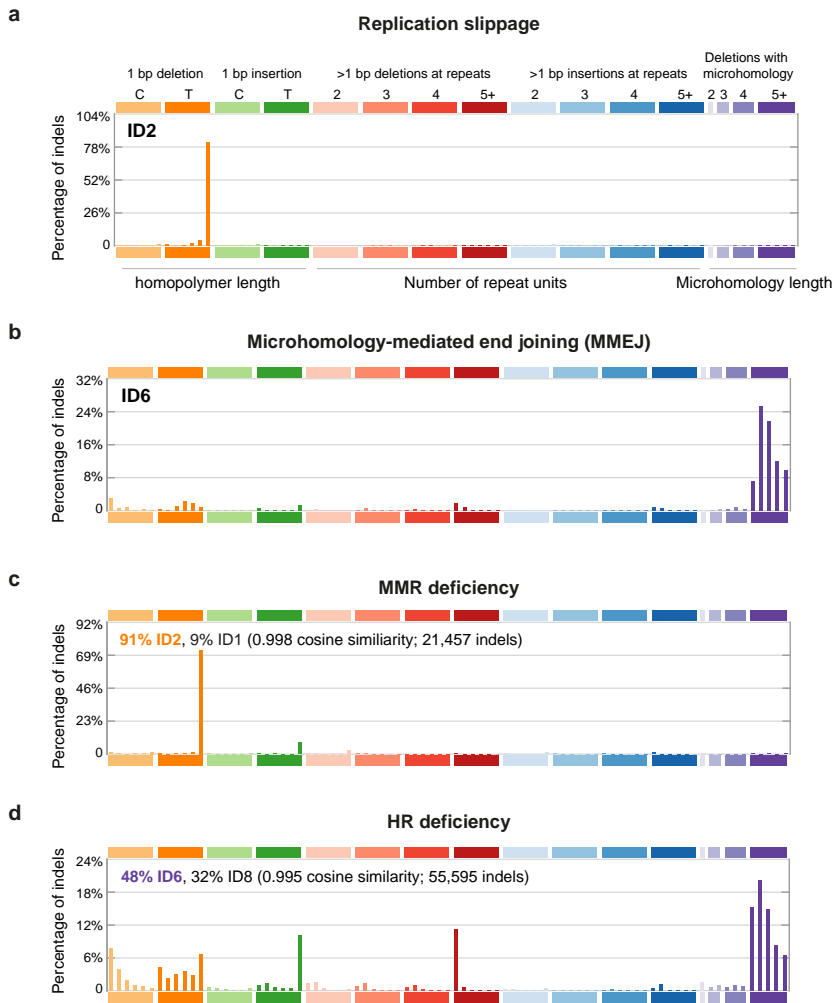


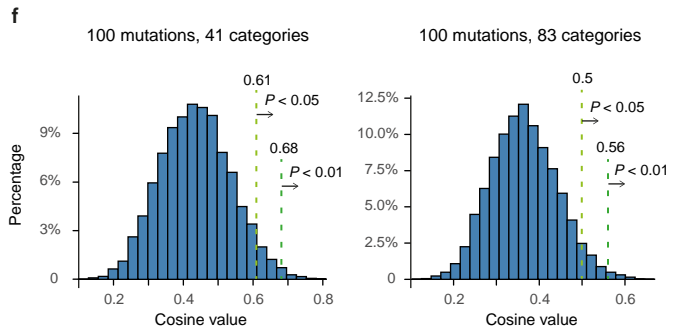
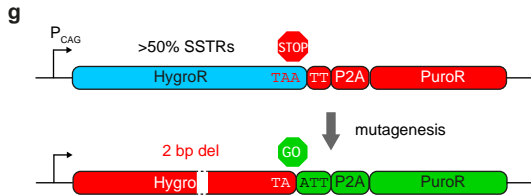
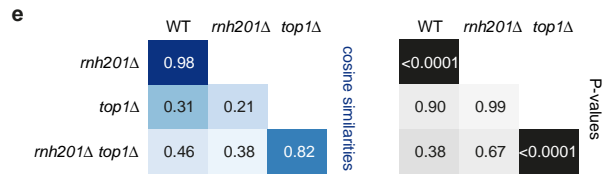
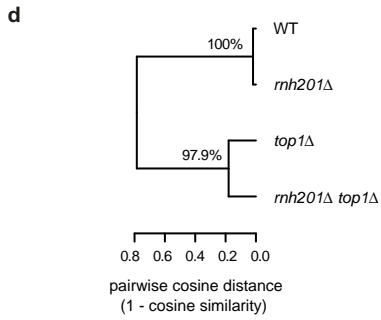
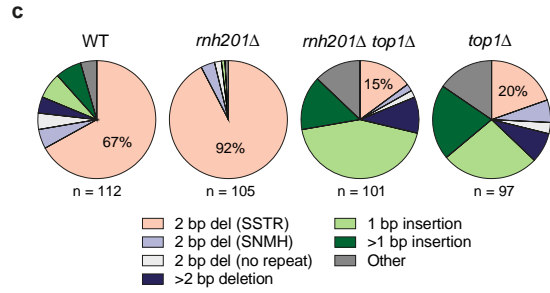
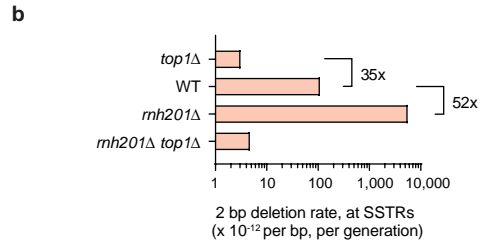
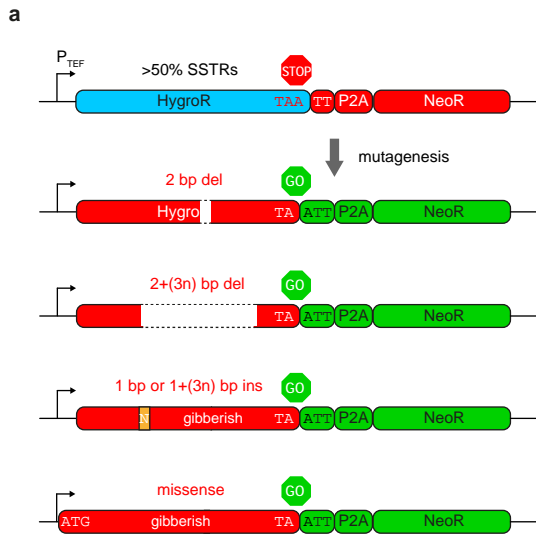


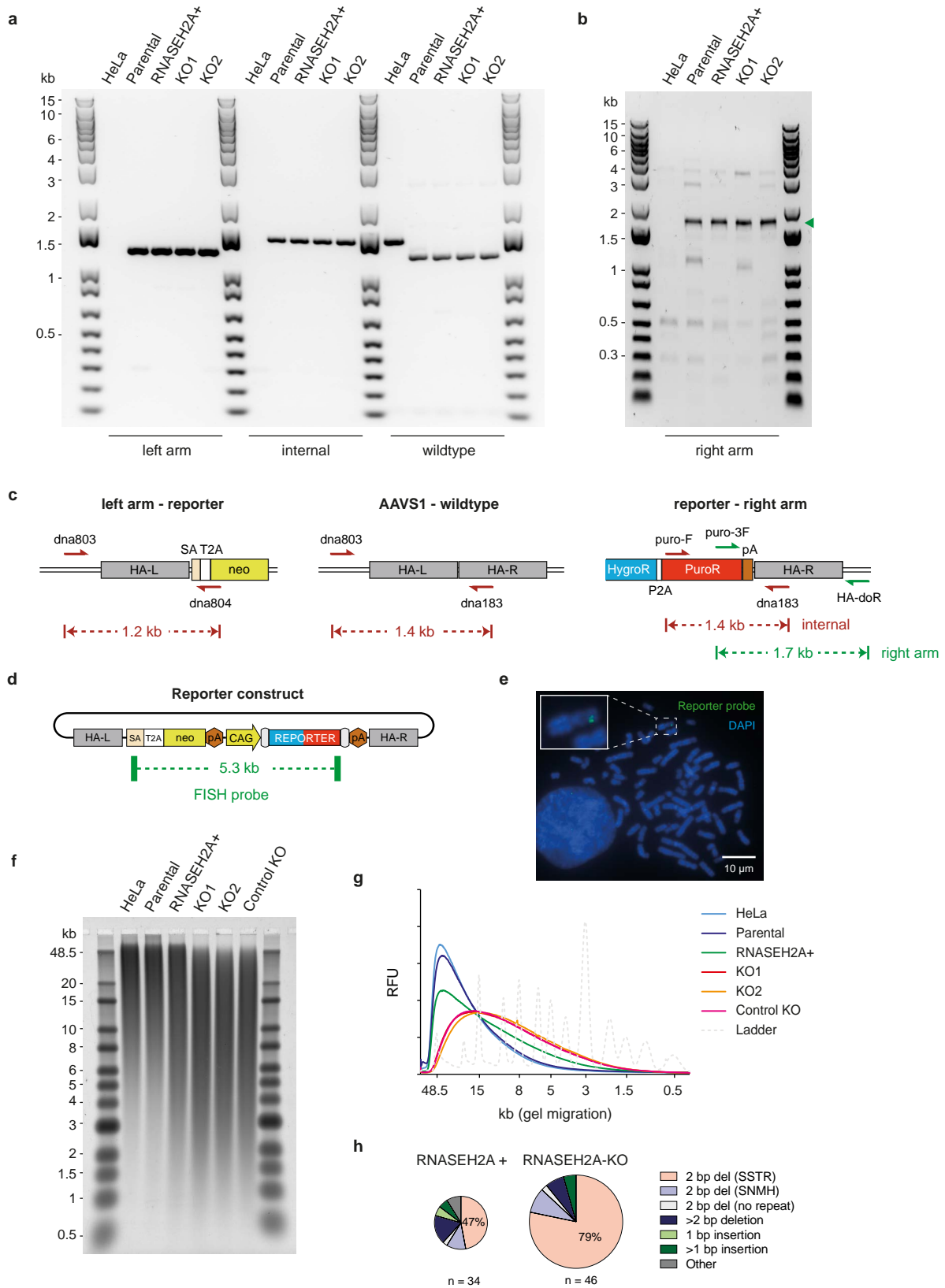


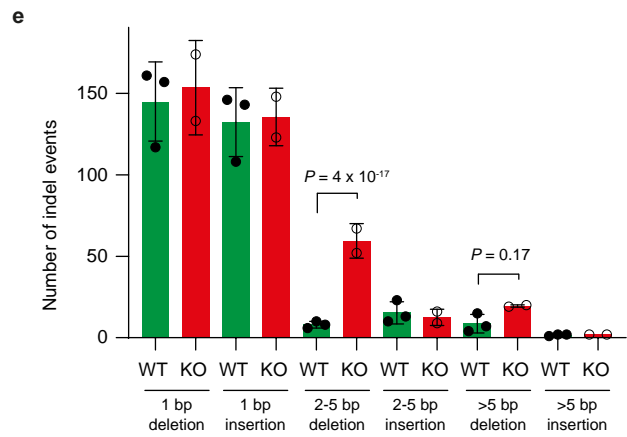
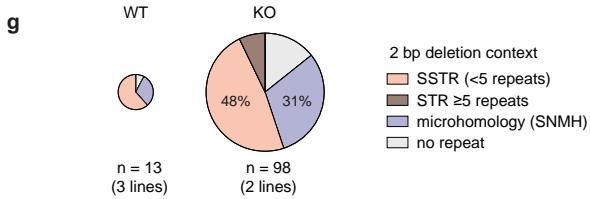
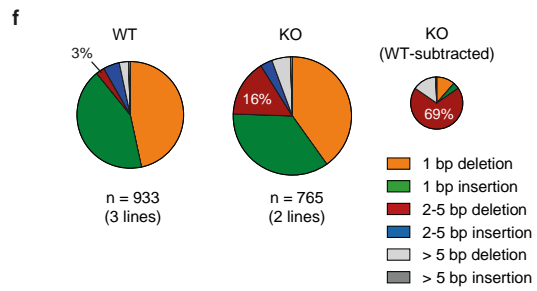
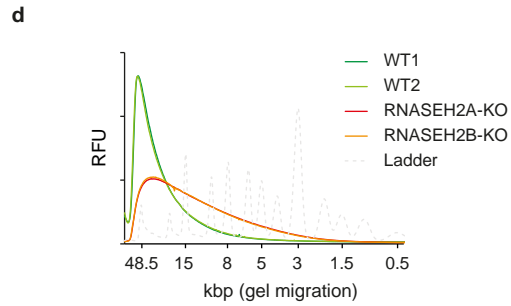
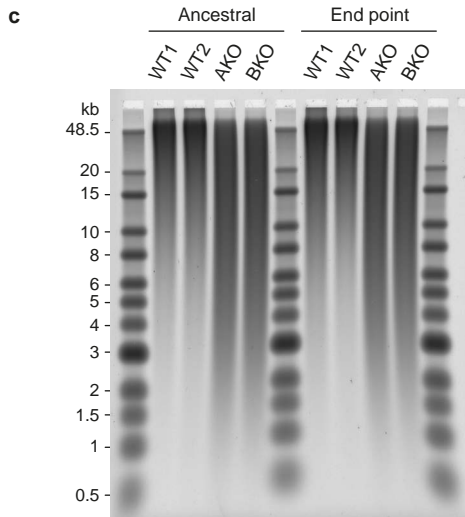
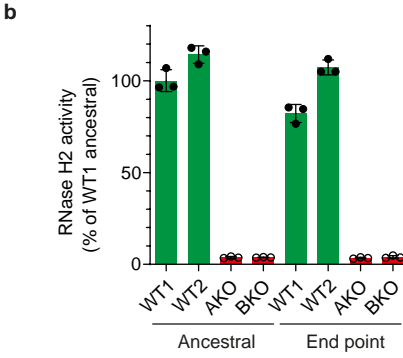
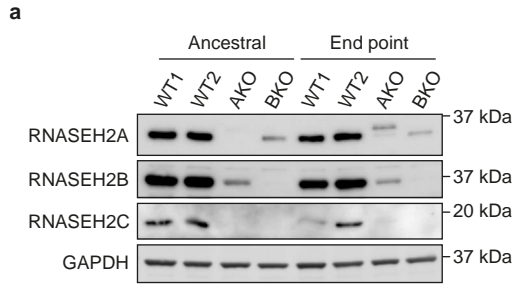


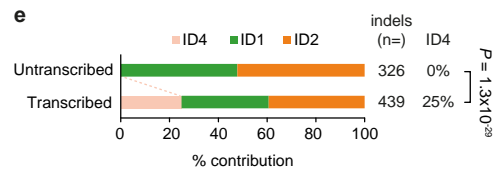
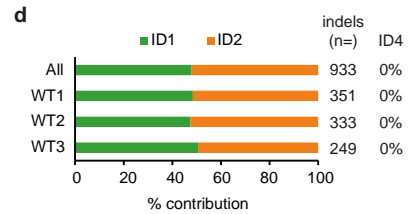
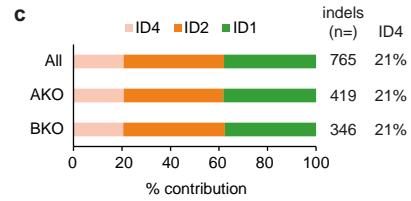
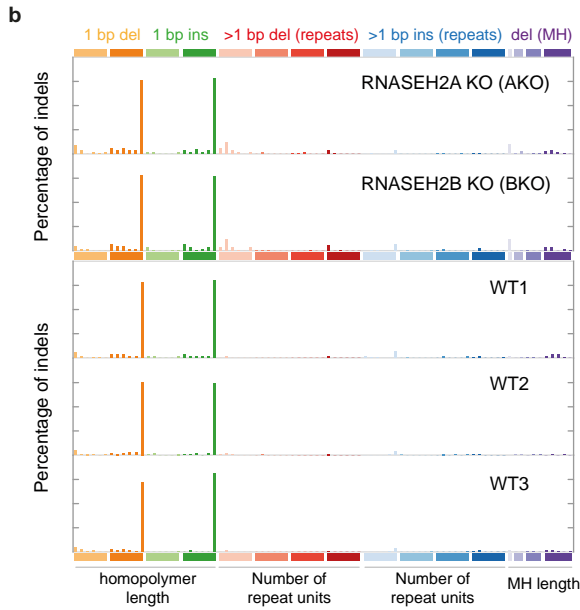
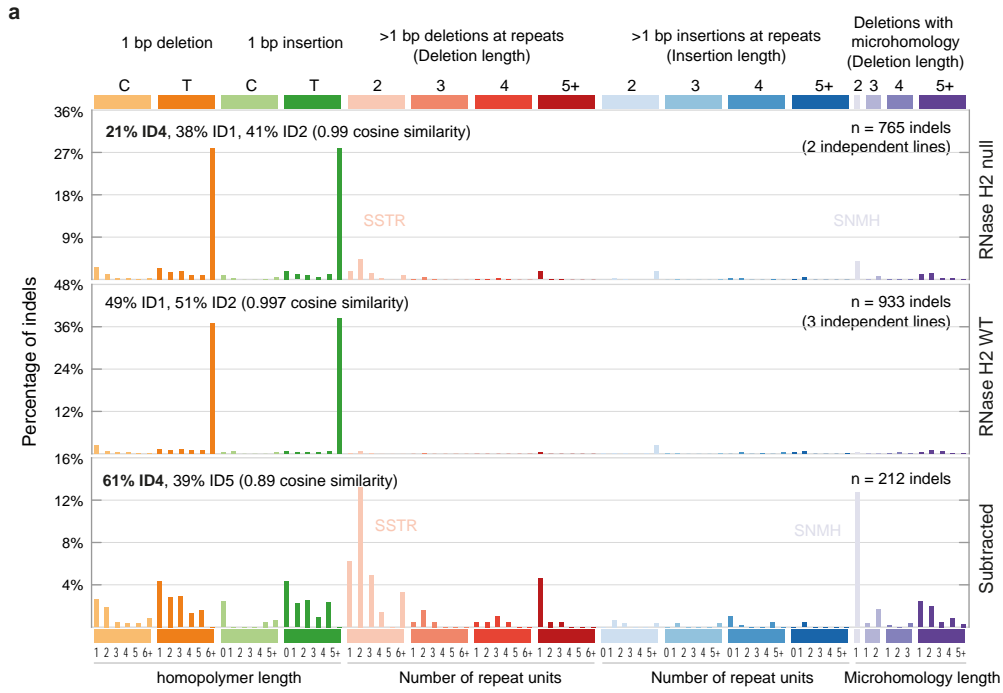


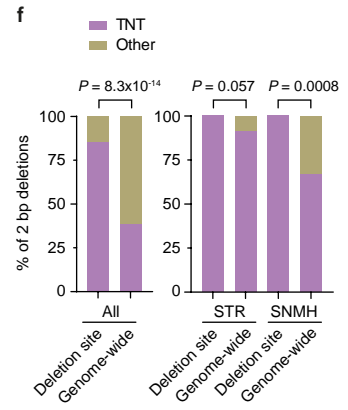
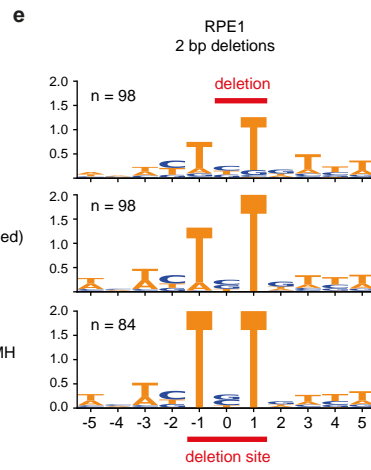
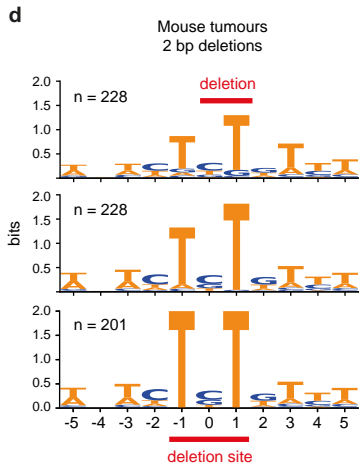
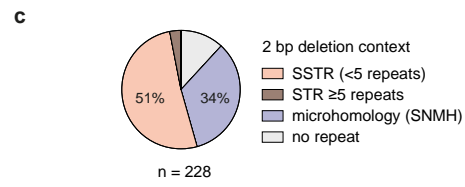
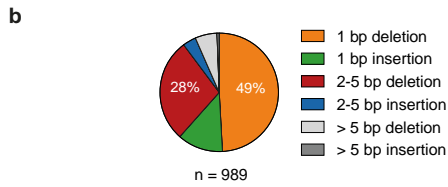
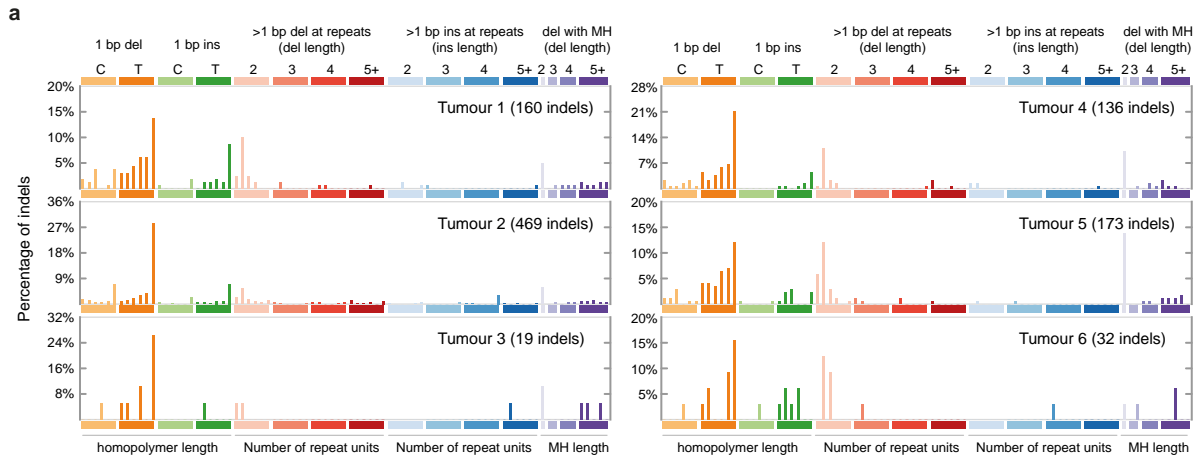


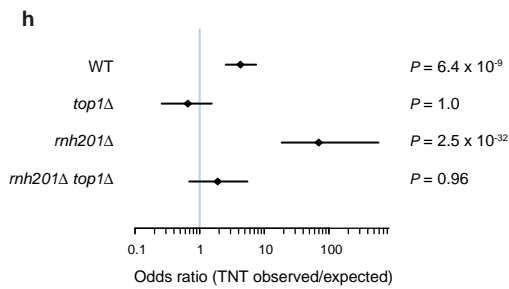
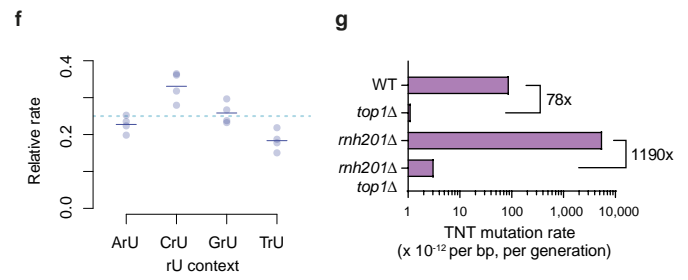
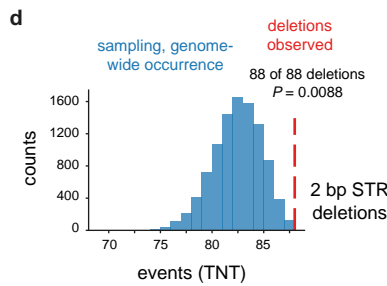
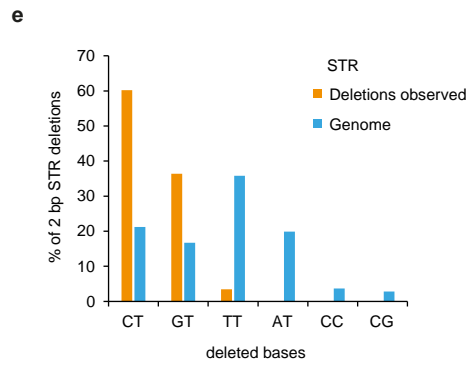
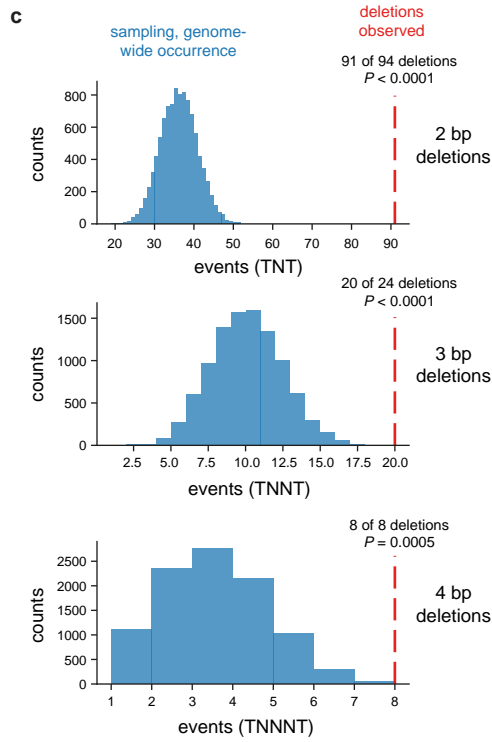
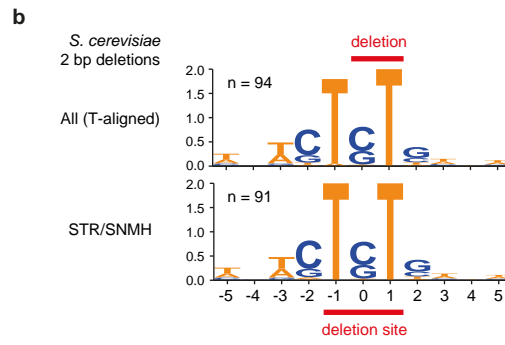
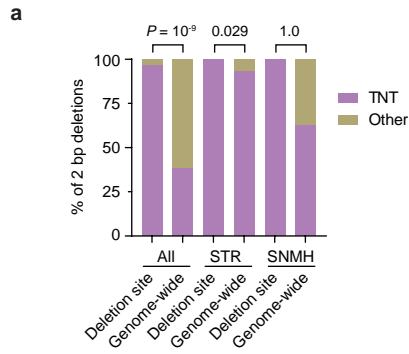


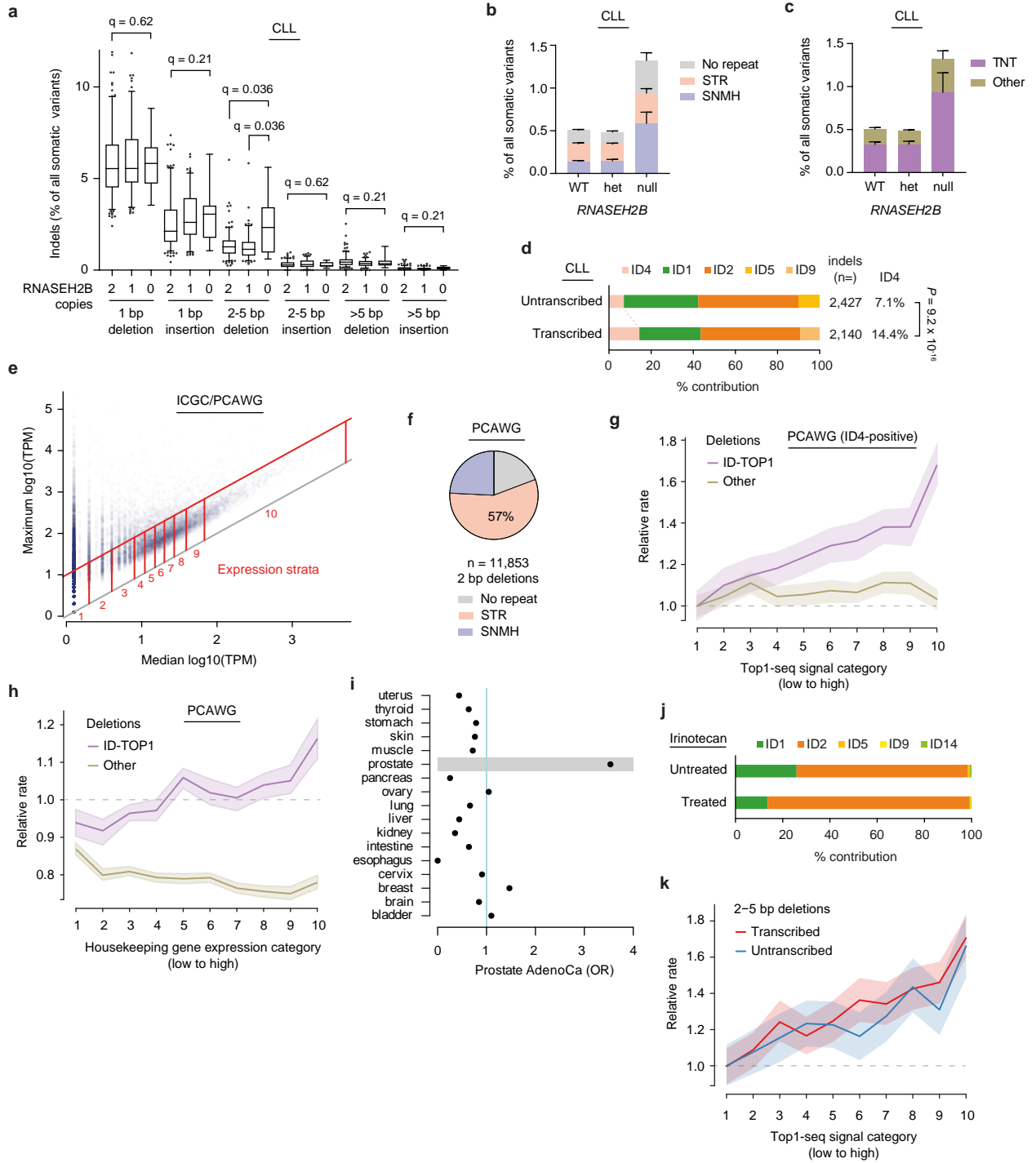


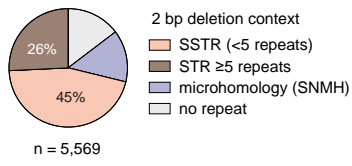
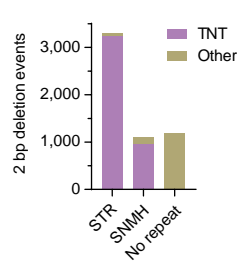
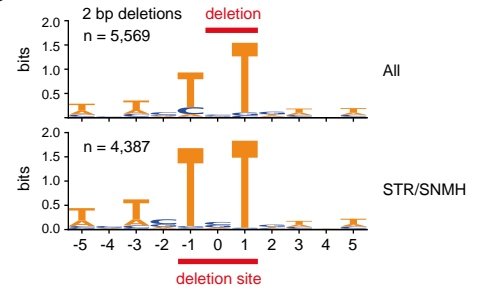
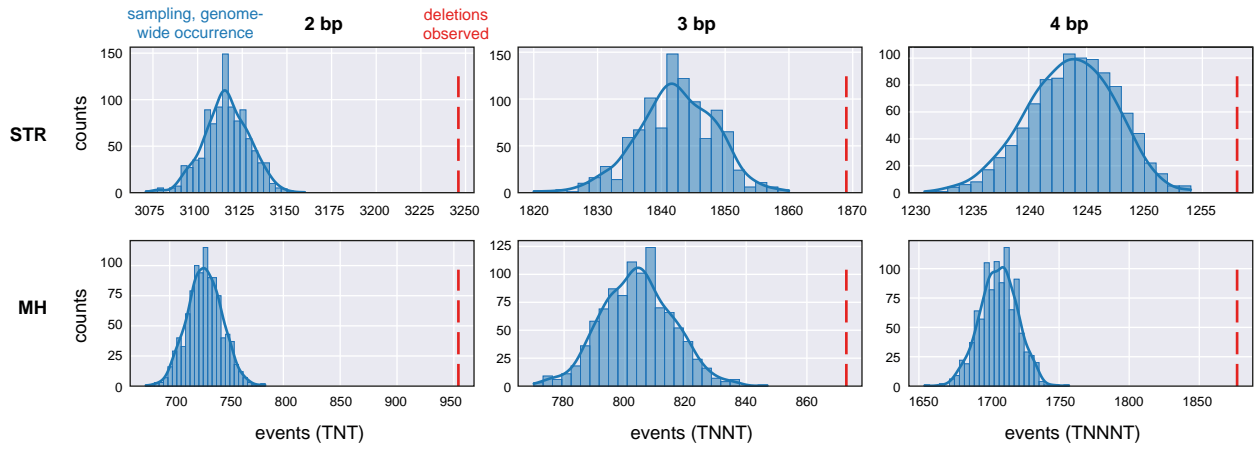










a**b****c****d****e**